

# The use of modeling and suspended sediment concentration measurements for quantifying net suspended sediment transport through a large tidally dominated inlet

Li H. Erikson <sup>a,\*</sup>, Scott A. Wright <sup>b</sup>, Edwin Elias <sup>c</sup>, Daniel M. Hanes <sup>d</sup>, David H. Schoellhamer <sup>b</sup>, John Largier <sup>e</sup>

<sup>a</sup> U.S. Geological Survey, Pacific Coastal and Marine Science Center, Santa Cruz, CA, USA

<sup>b</sup> U.S. Geological Survey, California Water Science Center, Sacramento, CA, USA

<sup>c</sup> Deltares, Delft, Netherlands

<sup>d</sup> Saint Louis University, Dept. of Earth and Atmospheric Sciences, MO, USA

<sup>e</sup> U.C. Davis Bodega Marine Laboratories, Bodega Bay, CA, USA

## ARTICLE INFO

### Article history:

Received 12 July 2012

Received in revised form 28 May 2013

Accepted 3 June 2013

Available online 13 June 2013

### Keywords:

inlet sediment flux

suspended sediment transport

estuaries

Delft3D

San Francisco Bay

## ABSTRACT

Sediment exchange at large energetic inlets is often difficult to quantify due complex flows, massive amounts of water and sediment exchange, and environmental conditions limiting long-term data collection. In an effort to better quantify such exchange this study investigated the use of suspended sediment concentrations (SSC) measured at an offsite location as a surrogate for sediment exchange at the tidally dominated Golden Gate inlet in San Francisco, CA. A numerical model was calibrated and validated against water and suspended sediment flux measured during a spring–neap tide cycle across the Golden Gate. The model was then run for five months and net exchange was calculated on a tidal time-scale and compared to SSC measurements at the Alcatraz monitoring site located in Central San Francisco Bay ~5 km from the Golden Gate. Numerically modeled tide averaged flux across the Golden Gate compared well ( $r^2 = 0.86$ ,  $p$ -value < 0.05) with 25 h low-pass filtered (tide averaged) SSCs measured at Alcatraz over the five month simulation period (January through April 2008). This formed a basis for the development of a simple equation relating the advective flux at Alcatraz with suspended sediment flux across the Golden Gate. Utilization of the equation with all available Alcatraz SSC data resulted in an average export rate of 1.2 Mt/yr during water years 2004 through 2010. While the rate is comparable to estimated suspended sediment inflow rates from sources within the Bay over the same time period (McKee et al., 2013–this issue), there was little variation from year to year. Exports were computed to be greatest during the wettest water year analyzed but only marginally so.

Published by Elsevier B.V.

## 1. Introduction

Large tidal estuaries located at the interface between rivers and the ocean provide a wealth of natural resources and are often an economic hub in many parts of the world. A quantitative understanding of sediment delivered to, stored within, and exported from an estuary is important for a number of issues including maintenance dredging of navigation channels, sand mining, light availability for primary productivity, creation and sustainability of tidal wetlands, and the transport of particle-bound nutrients and contaminants (Teeter et al., 1996; Zedler and Callaway, 2001). Although an estuary provides a readily definable control volume where point sources and sinks exist in the form of rivers and the open ocean, it is difficult to determine sediment influx to the system and net flux at the estuary–ocean boundary. This is particularly true for large tidal inlets in regions of modest to high tide ranges where it is not physically or

economically feasible to continuously monitor sediment flux, and exchange is complicated by variations in bathymetry, topography, and density driven flows.

San Francisco Bay is the largest estuary on the U.S. West Coast (Conomos et al., 1985), with an aerial extent of 1200 km<sup>2</sup> and is one example where these issues arise. Sediment exchange between the Bay and Pacific Ocean, which occurs across the > 1.5 km wide tidally dominated Golden Gate inlet, is the least well characterized component of the of the sediment budget. On the basis of conservation of mass, net suspended sediment flux through the Golden Gate has been inferred by accounting of sediment inflows to the Bay and change in sediment storage within the Bay (Ogden Beeman and Associates, 1992; Schoellhamer et al., 2005). Net suspended sediment flux was consistently shown to be seaward with net annual rates decreasing from 5 Mt/yr (million metric tons per year) during the 1990–1995 period to 4.2 Mt/yr for years 1995–2002 (Schoellhamer et al., 2005). Inferences of flux through the Gate can also be made from measurements of water discharge and salinity as a surrogate for scalar components obtained by Fram et al. (2007) and Martin et al. (2007). In that

\* Corresponding author. Tel.: +1 831 460 7563.

E-mail address: [lerikson@usgs.gov](mailto:lerikson@usgs.gov) (L.H. Erikson).

study, a series of transects across the Golden Gate were made with a boat-mounted ADCP and a suite of towed instruments. The results showed that both density gradients and bathymetry influence ocean–estuary exchange and that overall, exchange of salinity was far less than prior studies had shown (Parker et al., 1972; Largier, 1996). From the measurements they determined that chlorophyll flux was dominated by tidal pumping, accounting for 64–93% of the net dispersive flux. Similar to the sediment budget studies, net advective flux was shown to be seaward.

Efforts directly aimed at quantifying suspended flux through the Golden Gate were done with the use of numerical model simulations to define sediment transport pathways and in situ measurements for estimation of total net suspended flux over two weeks (Hauck et al., 1990; Teeter et al., 1996). Annual net flux was extrapolated from the two-week measurement campaign encompassing a neap–spring cycle coincident with low freshwater input to the Bay. A short-coming of that approach is that extrapolating the results to encompass much longer time-periods neglects variations in seasonal patterns of sediment delivery and changing hydrology in response to freshwater inputs and annual tide cycle deviations. In this study, the approach of Teeter et al. is expanded upon and the use of measured suspended-sediment concentrations, along with a simple tidal current model is investigated as means of estimating the suspended sediment flux through the Golden Gate. The use of surrogates to quantify sediment flux through estuarine channels has been done previously for smaller and less energetic embayments (Ganju and Schoellhamer, 2006), but not for large estuaries such as San Francisco Bay. To account for the large geographic scope of San Francisco Bay and high-energy exchange through the Golden Gate, a numerical model simulating sediment transport in the Bay–ocean system was calibrated against measured suspended sediment flux across the inlet. The calibrated and validated model was run for a five month time-period coincident with available suspended sediment concentration (SSC) measurements recorded at Alcatraz Island. Simulation results were then used to derive an equation relating measurements at the Alcatraz monitoring station along with the influence of upstream freshwater loading and sediment flux through the Golden Gate.

The remainder of this paper describes the study site, outlines the data and methods employed, presents the results, and concludes with a discussion and conclusion. In the results section, measurements obtained at the Golden Gate are first presented in order to highlight the variability of water and sediment flux across the channel. Numerical model results are then compared to the flux measurements at the Gate and used to explain some of the variability noted in the observations. The third and final results sub-section presents SSC values from the continuous Alcatraz monitoring station, a model for estimation of currents at Alcatraz, and the equation relating Alcatraz SSC and currents to suspended flux at the Golden Gate.

## 2. Study site

The San Francisco Bay Coastal System is a complex coastal–estuarine system, with often highly energetic physical forcing, including spatially and temporally variable wave, tidal current, wind, and fluvial forcing. The open coast at the mouth of San Francisco Bay is exposed to swell from almost the entire Pacific Ocean, with annual maximum offshore significant wave heights ( $h_s$ ) typically exceeding 8.0 m, and mean annual  $h_s = 2.5$  m (Scripps Institution of Oceanography, 2012). Inside the Bay, wave forcing is less important, except on shallow Bay margins where local wind-driven waves, and occasionally open ocean swell can induce significant turbulence and sediment transport (Talke and Stacey, 2003).

Tides at Fort Point (NOAA/Co-ops station 9414290) are mixed, semi-diurnal, with a maximum tidal range of 1.78 m (MLLW–MHHW, 1983–2001 Tidal Epoch). Due to the large volume of the

Bay (spring tidal prism of  $2 \times 10^9$  m<sup>3</sup>) currents are strong at the Golden Gate constriction where peak ebb tidal velocities exceed 2.5 m/s and peak flood currents reach 2 m/s (Rubin and McCulloch, 1979; Barnard, 2007). The strongest tidal currents throughout the other sub-embayments are focused in the main tidal channels. Though far less dominant physical forcing mechanisms compared to tidal forcing, which causes most of the estuarine mixing (Cheng and Smith, 1998), gravitational circulation and freshwater input (1% of the daily tidal flow, ~19% during record flow) are occasionally important during strong stratification events, with the effects most pronounced in the sub-embayments most distal from the inlet mouth (Monosmith et al., 2002).

Freshwater discharge into the Bay is predominantly from the Central Valley watershed, fed through San Joaquin–Sacramento Delta, which enters the Bay at Mallard Island (Figs. 1 and 2B) and historically supplied 83–86% of the fluvial sediments that enter the Bay (Conomos, 1979; Porterfield, 1980; Smith, 1987). Inputs from the Delta are controlled by water operations and reservoir releases, which are strictly managed during the low-flow season (~May–November) to keep the 2- $\psi$  isohaline seaward of the Delta. During wet winters, turbid water plumes from the Central Valley watershed have extended into South Bay (Carlson and McCulloch, 1974) and out past the Golden Gate (Ruhl et al., 2001).

The majority of sediment delivered to the Bay has historically been from the Delta (Porterfield, 1980), with nearly all (87–99%) of it in suspension (Schoellhamer et al., 2005; Wright and Schoellhamer, 2005). In recent years, suspended sediment loads from the Delta have diminished in response to ceased hydraulic mining of the 19th Century and other factors (Wright and Schoellhamer, 2004; Singer and James, 2008; McKee et al., 2013–this issue) causing the relative importance of loads from the small 250+ local tributaries to increase. These local watersheds may now account for ~61% of the total suspended load entering San Francisco Bay (McKee et al., 2013–this issue), but are typically episodic such that 90% of the total annual sediment load is released during only a few days (Kroll, 1975; McKee et al., 2006).

San Francisco Bay sediment consists primarily of silts and clays in South, San Pablo, and Suisun Bays and the shallow waters of Central Bay (Fig. 1), while sands dominate in the deeper parts of Central, San Pablo and Suisun Bays and in Carquinez Strait (Conomos and Peterson, 1977). Sediment grain sizes range from 2  $\mu$ m to 430  $\mu$ m in the northern embayments (Locke, 1971; Jaffe et al., 2007), from 62  $\mu$ m to 350  $\mu$ m in Central Bay (Chin et al., 2010; Barnard et al., 2011), and are on the order of 290  $\mu$ m at the open coast (Barnard et al., 2007). Due to strong tidal currents, the 113 m deep channel floor at the Golden Gate is void of sediment with exposed bedrock.

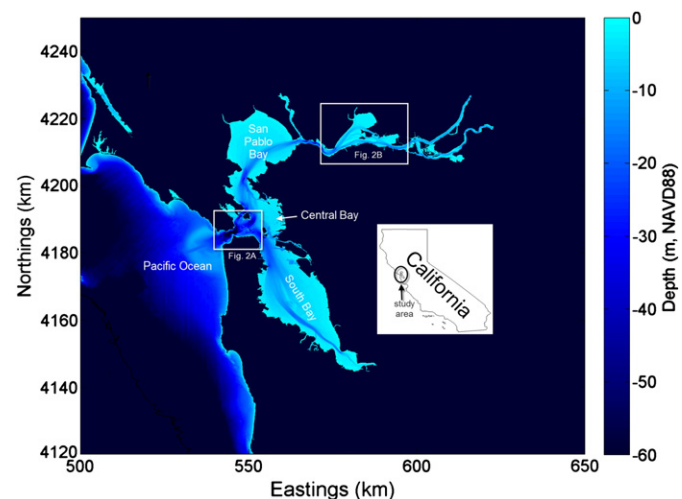


Fig. 1. Site study map showing San Francisco Bay, North and Central Bays, and the Sacramento/San Joaquin Rivers (Delta).

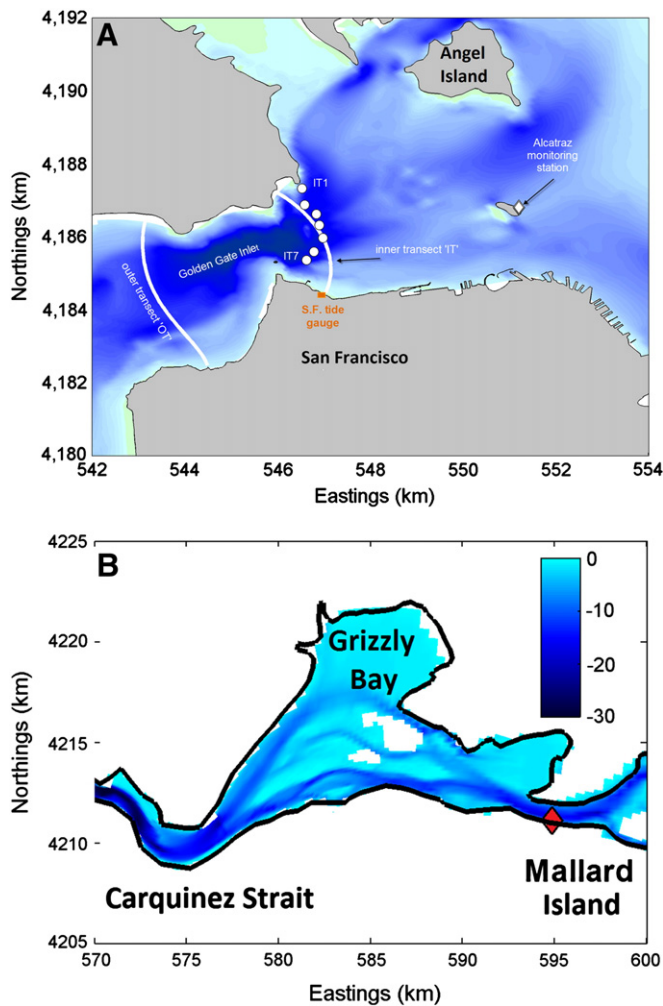


Fig. 2. Studied areas of suspended sediment flux; (A) Golden Gate inlet at the ocean-estuary interface, and (B) Mallard Island at the constriction between the Delta and remainder of San Francisco Bay. Depth shading in A is the same as in Fig. 1.

### 3. Data and methods

#### 3.1. SSC monitoring

The U.S. Geological Survey operates continuous monitoring of SSC on the northeast side of Alcatraz Island (N37.82722, W122.42167; Fig. 2A) 5 km from the Golden Gate inlet and a second one at the California Department of Water Resources Mallard Island Compliance Monitoring Station (N38.042778, W121.91917; Fig. 2B) located between the confluence of the Delta and Suisun Bay in the northern reaches of S.F. Bay (Buchanan and Lionberger, 2006). The sonde at Alcatraz is positioned approximately mid-way in the water column at ~3 m below mean sea level and consists additionally of a conductivity sensor for inference of salinity concentrations. Two optical sensors continuously monitor SSC in the upper and lower parts of the water column at Mallard Island (total water depth ~8.8 m). In this study, SSC measurements from the upper sensor at Mallard Island were used to represent suspended sediment influx to San Francisco Bay from the Delta region. The upper sensor was used in an effort to reduce the contribution of re-suspended and bed-load material in the measurements. With the exception of data drop-outs due to instrument malfunction or bio-fouling, the Alcatraz and Mallard Island monitoring sites have been operational since November 2003 and February 1994, respectively. Instruments at both sites log one measurement every 15 min. For details on sensor types, calibration, and accuracy see Buchanan and Lionberger (2006).

#### 3.2. Freshwater inflows

Freshwater inflows to San Francisco Bay were estimated with the Dayflow model (CDWR, 2012). Dayflow provides an idealized, unidirectional flow value that is the net water balance of all freshwater inputs and outputs to the Sacramento/San Joaquin River Delta. Daily averaged values between 1956 and 2010 show that maximum flows typically occur during the winter and spring months (January through April) in response to high precipitation events and snow melt, and on average range from 1000 m<sup>3</sup>/s to >2000 m<sup>3</sup>/s with a peak in late February to early March (Fig. 3). Delta inflow rates were critically low (~500 m<sup>3</sup>/s; dashed line and dark shaded area in Fig. 3) in water year (WY) 2008, October 01 2007–September 30 2008, and during the Golden Gate sediment flux monitoring period in January 2008 discussed in the next section. A week prior to the flux measurements, 'normal' inflow rates of 1450 m<sup>3</sup>/s were reached for a brief time.

#### 3.3. Vertical profiles of water column properties at the Golden Gate

Vertical profiles of temperature, salinity, velocity and acoustic backscatter (600 kHz RDI ADCP), and volumetric suspended-sediment concentration and grain size (Sequoia Scientific LISST-100X) were collected at seven locations along a transect just inside the Golden Gate (Inner Transect, IT, Fig. 2A, Table 1). Profiles were collected during a neap tide on 17 Jan 2008 and during a spring tide on 24 Jan 2008 (Fig. 4). Tables 2A and 2B summarize the along channel currents ( $u_{ac}$ ), grain size ( $g_s$ ), salinity, and temperature ( $S$  and  $T$ ) measured at the seven stations for neap (Table 2A) and spring (Table 2B) tides. Point measurements of suspended-sediment concentration (by mass) were made in conjunction with the 17 Jan 2008 profiling in order to estimate floc density and provide a conversion from LISST volume concentration to mass concentration. A USGS P-61 sampler (Edwards and Glysson, 1999) was used to collect 20 samples co-located with LISST profiles, ranging in depth from 3 m to 30 m. Comparison of the P-61 and LISST concentrations (Fig. 5A) yielded a floc density of 1.26 g/cm<sup>3</sup> which is comparable to other published estimates for San Francisco Bay (Krank and Milligan, 1992).

#### 3.4. Moving-boat velocity and backscatter profiling along lateral transects

Three-dimensional velocity and acoustic backscatter data were collected (600 kHz RDI ADCP) from a moving boat (DGPS for positioning) along two transects, one just inside (IT) and one just outside of the Gate (OT) (Fig. 2A). Neap tide measurements were made on Jan 16 (outer) and Jan 17 (inner) while spring tide measurements were made on Jan 23 (outer) and Jan 24 (inner). The water and boat velocity data were used to compute the total water flux through the cross-section using standard techniques for computing discharge from moving-boat ADCP data (Simpson, 2001). Suspended-sediment flux through the cross-section was computed from a similar technique that incorporates calibrated backscatter data from the ADCP. Backscatter intensity data were corrected for beam spreading and water absorption (attenuation due to sediment was determined to be small), then calibrated to SSC using the vertical profile data described above. Concurrent backscatter and calibrated LISST profiles were used to generate the backscatter-SSC calibration (log scale, see e.g. Gartner, 2004) shown in Fig. 5B. This calibration was used to convert backscatter data from the moving boat transects to SSC. The total suspended-sediment flux through the cross-section was then computed by multiplying SSC and velocity in each ADCP bin, then integrating these sediment fluxes over the cross-section in the same manner as for the water flux measurements.

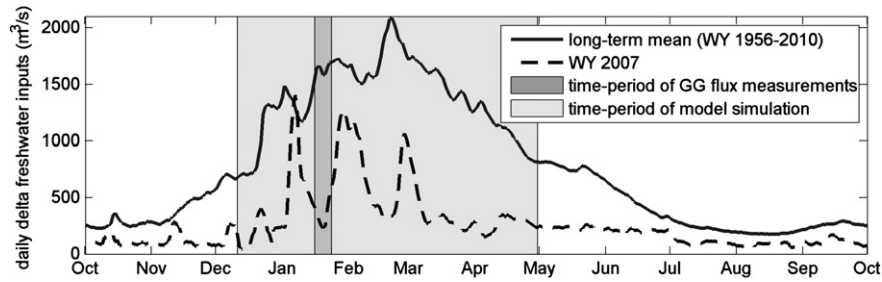


**Fig. 3.** Net freshwater inflows from the Sacramento/San Joaquin River Delta to San Francisco Bay (California Department of Water Resources, 2012). Darker gray area highlights the time-period in water year (WY) 2008 when flux measurements at the Golden Gate were obtained for this study; lighter gray shading indicates time-period of model simulation. Compared to the long-term mean (solid line), freshwater inputs were low during the flux measurements.

### 3.5. Numerical modeling

Suspended sediment flux measurements obtained in January 2008 (Sections 3.3 and 3.4) coincided with relatively low seas and swell (max significant wave heights = 2.5 m at the SF Bar buoy, CDIP) and calm meteorological conditions (max winds < 5 m/s, NDBC) and hence only tidal forcing, freshwater, and sediment inputs were used as boundary conditions to model sediment flux through the Golden Gate.

The numerical model Delft3D was used to simulate water and sediment exchange at the Golden Gate (Lesser et al., 2004; Deltares, 2011). The Delft3D package is a modeling system that consists of a number of integrated modules; the ones relevant to this work allow for the simulation of hydrodynamic flow by solving the shallow water equations, and transport of salinity and sediment by solving the advection–diffusion equation.

Given the large spatial extent of the San Francisco Bay system, the model was divided into five two-way coupled domains of varying resolution thus enabling parallel computing and reducing computation time (Fig. 6). Grid resolution ranged from ~50 to 100 m at the Golden Gate inlet and from 100 m to >500 m in the northern reaches of Suisun Bay. The Delta was highly schematized as the primary goal was to provide storage of the tidal prism. Tidal variations were driven at the open boundaries of the large-scale ocean domain that extended out past the continental shelf. A total of 12 tidal constituent amplitudes and phases ( $M_2$ ,  $S_2$ ,  $N_2$ ,  $K_2$ ,  $K_1$ ,  $O_1$ ,  $P_1$ ,  $Q_1$ , MF, MM,  $M_4$ ,  $MS_4$ , and  $MN_4$ ) were applied at the open boundary with initial estimates obtained from the TOPEX7.2 global tidal model (Egbert et al., 1994; Egbert and Erofeeva, 2002). Hydrodynamic aspects of the model were calibrated and validated against >30 tide stations throughout the Bay and water flux measurements obtained along the inner and outer transects across the Golden Gate described previously. Details of the numerical modeling approach used in this study, including hydrodynamic model calibration and validation, can be found in Elias and Hansen (2012).

All domains were run in a depth averaged mode (2DH). This approach assumes that flows at the Golden Gate and all other areas are vertically well-mixed and not strongly stratified; a reasonable assumption given that the model simulations were done for a critically

dry water year and that there was little vertical variation in measured salinity. If the water column was actually strongly stratified then the 2D model would presumably have significant discrepancies in the predicted fields of both velocity and suspended sediment concentration. Typically the vertical velocity gradients would be larger for stratified flows, and the suspended sediment distribution could be influenced by flocculation processes if there was a sharp interface between fresh and brackish water.

Four sediment fractions were simulated in the model; two non-cohesive (sand) and two cohesive. Based on measured grain size distributions at the Golden Gate and previous measurements within Central Bay and outer coast, median sand-sized particles of 200  $\mu\text{m}$  and 350  $\mu\text{m}$  were simulated. A specific density of 2650  $\text{kg}/\text{m}^3$  and dry bed density of 1600  $\text{kg}/\text{m}^3$  was assumed for all sand fractions; all sand transport calibration parameters were kept at the default values. Sand fraction transport was modeled with the van Rijn TR2004 formulation, which has been shown to successfully represent the movement of non-cohesive sediment ranging in size from 60  $\mu\text{m}$  to 600  $\mu\text{m}$  (Van Rijn, 2007).

Transport of the cohesive mud fractions were modeled with the Krone and Ariathurai–Partheniades formulations (Krone, 1962; Ariathurai, 1974). The critical shear stress for deposition ( $\tau_{crd}$ ) was set to 1000  $\text{N}/\text{m}^2$ , which effectively implied that deposition was a function only of concentration and fall velocity (Wintwerp and Van Kesteren, 2004). The critical shear stress for erosion ( $\tau_{cre}$ ), fall speed velocity ( $w_s$ ), and erosion rate constants ( $M$ ) were treated as calibration parameters. Values in the range of  $0.1 \text{ N}/\text{m}^2 < \tau_{cre} < 0.4 \text{ N}/\text{m}^2$ ,  $0.09 \text{ mm}/\text{s} < w < 1.01 \text{ mm}/\text{s}$ , and  $5 \cdot 10^{-5} \text{ kg}/\text{m}^2/\text{s} < M < 2 \cdot 10^{-4} \text{ kg}/\text{m}^2/\text{s}$  were tested based on previous laboratory and modeling studies (Mehta, 1986; Teeter, 1986; Kineke and Sternberg, 1989; Krank and Milligan, 1992; Ganju and Schoellhamer, 2009; van der Wegen et al., 2011a,b). Characteristic parameters of the mud fractions were determined by running numerous simulations with varying sediment size and minimizing observed–modeled differences; the resulting parameters are listed in Table 3. A mid-range dry bed density of 850  $\text{kg}/\text{m}^3$  was assigned to both cohesive fractions (Porterfield, 1980). Based on recent field measurements (Manning and Schoellhamer, 2013–this issue), fall speed velocities were kept constant under all salinity concentrations and flocculation was considered to be negligible.

Bed composition maps were generated following guidelines outlined by van der Wegen et al. (2011a,b). In that approach, initial bed composition is estimated by defining sediment availability throughout the domain and then running the model over long time periods to distribute sediments over the domain using prevailing hydrodynamic conditions. The resulting bed composition is then used as the initial condition. In this study, bed thickness maps were constructed from measurements summarized by Chin et al. (2004) and assuming 6 m in areas void of observations. A single layer was used, such that all fractions eroded and deposited onto the same layer. Initial estimates of bed composition were assumed to consist of 100% sand in the ocean domain and at the Golden Gate inlet, 6% cohesive and 94% sand in Central Bay and central channels of north

**Table 1**  
Location and water depth at stations sampled along the inner transect (IT).

Station ID	Lon (DD)	Lat (DD)	Water depth (m)
IT1	–122.47126	37.83215	32.5
IT2	–122.47064	37.82814	51.9
IT3	–122.46781	37.82580	57.1
IT4	–122.46712	37.82309	56.5
IT5	–122.46621	37.81988	50.5
IT6	–122.46843	37.81651	34.9
IT7	–122.47033	37.81450	30.9

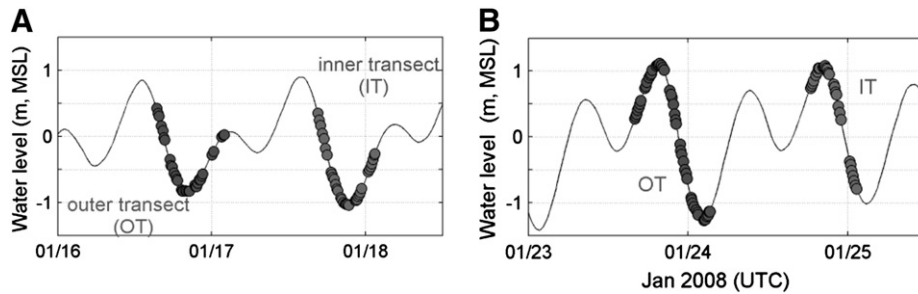


**Fig. 4.** Time and tidal stage of field measurements obtained during (A) neap and (B) spring tides. Circles indicate times when the vessel was stopped and instrumentation was dropped to measure water quality parameters throughout the water column. ADCP transects were run continuously during the four measurement periods.

and south bays, and 80% and 20% cohesive and sand in the remaining regions of the north and south bays, respectively. The model was then run to simulate ~10 years of sediment re-distribution using a morphological acceleration factor (MorFac) of 100. The use of MorFac values is based on the idea that morphologic changes take place over much longer time periods than hydrodynamic changes and as such, sediment fluxes to and from the bed can be multiplied by a constant MorFac at each morphologic time step in order to decrease the computation time of long-term simulations (Lesser et al., 2004; Roelvink, 2006).

Volumetric Delta flow rates and SSC measurements from the Mallard Island upper gauge were prescribed at the model boundary near Mallard Island to provide daily advective flux of sediment into the model domain. Measured SSCs were averaged over 24 h to

coincide with daily Dayflow values representing net freshwater volumetric flow rates from the Sacramento/San Joaquin Delta.

The numerical model was run from December 11, 2007 through April, 2008 to allow for model 'spin-up', encompass the time-period of Golden Gate flux measurements (Section 3.2 to 3.4), and capture some of the variations in measured SSC at Alcatraz. A three week spin up time was prescribed, so that only results from January 01 to April 30 2008 were used in the analysis.

### 3.6. Flux estimates at the surrogate monitoring site, Alcatraz

In developing a relationship between SSC at the Alcatraz monitoring site and sediment flux through the Golden Gate, estimates of flux rates at the Alcatraz monitoring site were evaluated. The relative

**Table 2A**

Water column properties measured along the inner transect during neap tide in January 2008.

St. ID	Parameter	Neap tide					
		Upper water column	Mid to upper water column	Mid to lower water column	Lower water column	Min	Max
IT1	$u_{ac}$ (cm/s)	93.1/–6.5	89.3/–10.4	78.4/–5.7	78.1/–10.8	–10.8	93.1
	SSC (uL/L)	27/54	30/57	28/66	29/72	27	72
	gs ( $\mu$ m)	31/41	35/44	40/48	41/58	31	58
	S (psu)	27.9/28.1	27.8/27.5	27.8/27.2	27.3/26.9	26.9	28.1
	T ( $^{\circ}$ C)	10.0/10.1	10.0/10.1	10.0/10.1	10.0/10.1	10	10.1
	$u_{ac}$ (cm/s)	125.0/–38.1	115.8/–42.7	102.4/–50.6	88.0/–63.7	–63.7	125
IT2	SSC (uL/L)	27/58	38/62	40/81	37/122	27	122
	gs ( $\mu$ m)	25/45	37/51	42/74	45/93	25	93
	S (psu)	28.5/29.5	30.8/28.7	30.1/28.5	29.9/28.0	28	30.8
	T ( $^{\circ}$ C)	10.0/10.2	10.3/10.1	10.2/10.1	10.1/10.1	10	10.3
	$u_{ac}$ (cm/s)	120.3/–82.5	112.1/–102.2	102.0/–113.7	96.3/–75.6	–113.7	120.3
	SSC (uL/L)	29/59	46/75	57/138	61/184	29	184
IT3	gs ( $\mu$ m)	42/46	42/50	43/64	41/63	41	64
	S (psu)	30.0/30.0	29.9/29.9	30.8/29.3	29.4/28.5	28.5	30.8
	T ( $^{\circ}$ C)	10.2/10.2	10.2/10.2	10.3/10.2	10.1/10.1	10.1	10.3
	$u_{ac}$ (cm/s)	90.2/–67.8	97.9/–68.3	100.2/–61.4	89.5/–37.4	–68.3	100.2
	SSC (uL/L)	33/71	47/77	57/108	68/121	33	121
	gs ( $\mu$ m)	42/48	47/58	55/77	50/63	42	77
IT4	S (psu)	31.0/29.9	30.9/29.8	29.6/29.3	29.5/28.5	28.5	31
	T ( $^{\circ}$ C)	10.3/10.2	10.3/10.2	10.2/10.2	10.2/10.1	10.1	10.3
	$u_{ac}$ (cm/s)	88.5/–78.3	94.6/–84.6	93.6/–66.7	81.4/–49.8	–84.6	94.6
	SSC (uL/L)	33/88	30/80	41/85	56/131	30	131
	gs ( $\mu$ m)	38/49	42/51	47/53	50/62	38	62
	S (psu)	30.8/29.9	30.8/29.8	30.3/29.6	29.8/29.4	29.4	30.8
IT5	T ( $^{\circ}$ C)	10.3/10.2	10.3/10.2	10.3/10.2	10.3/10.2	10.2	10.3
	$u_{ac}$ (cm/s)	85.4/17.7	82.0/7.8	73.5/–2.9	69.2/–1.5	–2.9	85.4
	SSC (uL/L)	69/77	85/91	97/124	98/144	69	144
	gs ( $\mu$ m)	43/47	40/52	45/56	45/55	40	56
	S (psu)	30.7/28.5	29.6/28.4	29.9/28.3	30.1/28.1	28.1	30.7
	T ( $^{\circ}$ C)	10.3/10.1	10.2/10.1	10.1/10.1	10.2/10.1	10.1	10.3
IT6	$u_{ac}$ (cm/s)	29.9/–13.0	35.6/–16.0	36.0/–11.8	45.9/–10.4	–16	45.9
	SSC (uL/L)	38/70	47/67	55/69	50/111	38	111
	gs ( $\mu$ m)	39/49	41/52	38/50	37/49	37	52
	S (psu)	30.8/30.7	30.7/30.7	28.8/30.7	28.7/30.5	28.7	30.8
	T ( $^{\circ}$ C)	10.3/10.3	10.3/10.3	10.1/10.3	10.1/10.3	10.1	10.3

Notes: Maximum and minimum values separated by a backslash (/). The upper, mid, and lower water columns each represent 25% of the total water depth as listed in Table 1. Reported SSC, gs, S, and T are those that were recorded in conjunction with the maximum ebb and flood velocities. Ebb flows are positive.

**Table 2B**

Water column properties measured along the inner transect during spring tide in January 2008. See Table 2A for description.

St. ID	Parameter	Spring tide					
		Upper water column	Mid to upper water column	Mid to lower water column	Lower water column	Min	Max
IT1	$u_{ac}$ (cm/s)	138.2/0.07	121.5/0.07	105.4/0.08	86.8/0.06	0.1	138.2
	SSC (uL/L)	64/124	65/123	67/134	68/143	64	143
	gs ( $\mu$ m)	32/37	32/39	36/38	36/42	32	42
	S (psu)	29.9/31.1	30.0/31.1	30.0/31.0	30.0/30.9	29.9	31.1
	T ( $^{\circ}$ C)	10.0/10.2	10.0/10.2	10.0/10.2	10.0/10.1	10.0	10.2
IT2	$u_{ac}$ (cm/s)	106.8/–53.2	119.9/–18.4	100.1/–34.1	73.6/–24.2	–53.2	119.9
	SSC (uL/L)	41/75	39/99	47/91	81/95	39	99
	gs ( $\mu$ m)	34/41	36/40	39/40	39/49	34	49
	S (psu)	30.4/31.4	30.1/31.3	30.0/31.3	30.9/30.7	30.0	31.4
	T ( $^{\circ}$ C)	10.1/10.2	10.0/10.2	10.0/10.2	10.1/10.1	10.0	10.2
IT3	$u_{ac}$ (cm/s)	106.8/–129.2	119.9/–127.1	100.1/–119.4	86.9/–109.1	–129.2	119.9
	SSC (uL/L)	32/63	42/63	52/85	59/97	32	97
	gs ( $\mu$ m)	34/37	35/39	39/41	39/47	34	47
	S (psu)	30.4/31.5	30.1/31.4	30.0/31.3	30.1/31.3	30.0	31.5
	T ( $^{\circ}$ C)	10.1/10.2	10.0/10.2	10.0/10.2	10.0/10.2	10.0	10.2
IT4	$u_{ac}$ (cm/s)	106.8/–166.2	119.9/–148.2	100.1/–125.7	64.1/–100.1	–166.2	119.9
	SSC (uL/L)	37/65	46/64	48/76	58/81	37	81
	gs ( $\mu$ m)	34/37	36/40	38/43	39/44	34	44
	S (psu)	30.4/31.3	30.1/31.2	30.0/31.0	29.7/31.0	29.7	31.3
	T ( $^{\circ}$ C)	10.1/10.2	10.0/10.2	10.0/10.2	9.9/10.2	9.9	10.2
IT5	$u_{ac}$ (cm/s)	112.0/–161.8	119.9/–163.9	100.1/–152.6	64.1/–121.9	–163.9	119.9
	SSC (uL/L)	38/80	40/80	40/86	45/81	38	86
	gs ( $\mu$ m)	37/39	39/41	39/51	39/44	37	51
	S (psu)	30.9/31.0	30.1/31.0	30.0/30.9	29.7/30.9	29.7	31.0
	T ( $^{\circ}$ C)	10.1/10.2	10.0/10.2	10.0/10.2	9.9/10.2	9.9	10.2
IT6	$u_{ac}$ (cm/s)	119.8/–15.3	119.9/0.04	100.1/0.20	87.6/0.19	–15.3	119.9
	SSC (uL/L)	44/90	60/96	62/104	62/108	44	108
	gs ( $\mu$ m)	35/39	36/44	38/45	38/47	35	47
	S (psu)	30.7/31.1	30.1/31.5	30.0/31.4	30.6/31.1	30.0	31.5
	T ( $^{\circ}$ C)	10.1/10.2	10.0/10.2	10.0/10.2	10.1/10.2	10.0	10.2
IT7	$u_{ac}$ (cm/s)	106.8/39.7	119.9/–29.5	100.1/–19.5	73.4/–6.6	–29.5	119.9
	SSC (uL/L)	40/102	53/97	64/129	68/166	40	166
	gs ( $\mu$ m)	35/40	37/41	39/41	39/43	35	43
	S (psu)	30.4/31.4	30.1/30.9	30.0/30.9	31.1/30.9	30.0	31.4
	T ( $^{\circ}$ C)	10.1/10.2	10.0/10.2	10.0/10.1	10.2/10.1	10.0	10.2

importance of different mechanisms contributing to the horizontal sediment flux ( $F$ ) can be estimated by averaging over a tidal cycle so that (Dyer, 1997):

$$F = \underbrace{[U][A][C]}_{(1)} + \underbrace{U'[A]C'}_{(2)} + \underbrace{U'A'[C]}_{(3)} + \underbrace{U'[A][C]}_{(4)} + \underbrace{[U]A'[C]}_{(5)} + \underbrace{[U][A]C'}_{(6)} + \underbrace{[U]A'C'}_{(7)} + \underbrace{U'A'C'}_{(8)} \quad (1)$$

where  $U$  denotes current velocity,  $A$  the cross-sectional area through which sediment passes, and  $C$  the SSC. The brackets denote cross-

sectional time averaged values, and the prime indicates deviations of instantaneous values from tidally averaged values (e.g.,  $C' = C - [C]$ ). Tide-averaging was done over 20, 25, 30, and 35 h in order to examine the different tidal time scales over which individual flux terms yield net balances. Low-pass filtering was attained with fourth order forward and reverse Butterworth low-pass filters with frequency cut-offs of 1/20 h, 1/25 h, etc.

The advective and dispersive flux terms (Eq. (1), terms 1 and 2, respectively) typically dominate the total flux, while Stokes drift contributes a smaller portion (Eq. (2), term 3) (Ganju and Schoellhamer, 2006). The advective flux term represents the Eulerian flux and

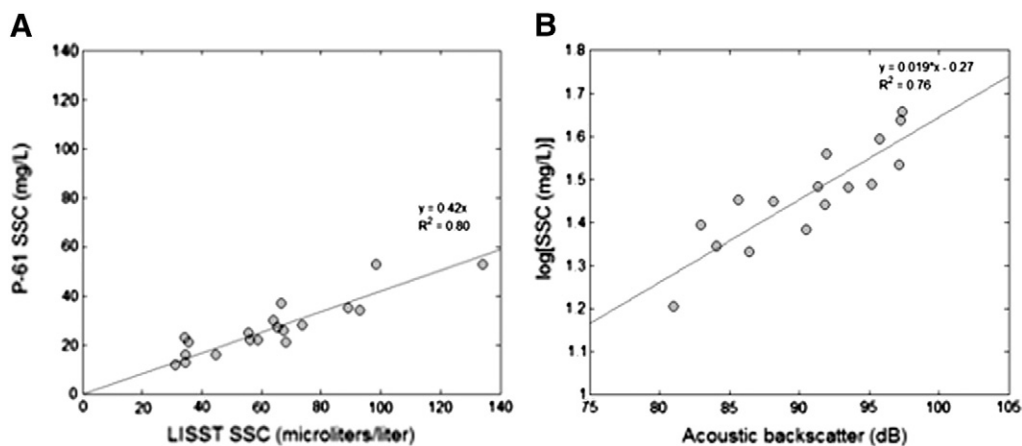


**Fig. 5.** Calibration curves for (A) mass SSC from water samples versus volumetric SSC from the LISST, and (B) mass SSC from the calibrated LISST versus acoustic backscatter from the ADCP.

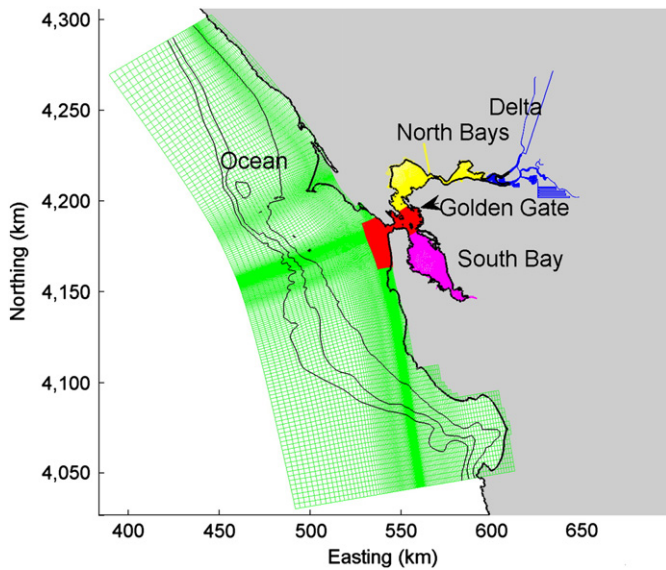


Fig. 6. Curvilinear grids used in the numerical model. A total of five two-way coupled domains were used: Ocean, Golden Gate, North Bays, Delta, and South Bay. Contours are the 100 m, 500 m and 1000 m isobaths.

quantifies the contribution of average discharge and concentration to the total flux, while the dispersive flux represents the correlation between velocity and sediment concentration fluctuations. Stokes drift characterizes the correlation between velocity and cross-sectional area. In this study, the ratio of the cross-sectional area at Alcatraz and the Golden Gate inlet was assumed to be constant, and therefore the Stokes drift term was excluded from further analysis. The remaining terms in Eq. (1) are usually negligible.

With the aim of developing an analytical approach to estimating flux at Alcatraz, a readily useable relationship to estimate currents at this site was required. Because the currents are tidally dominated, harmonic analysis of a velocity time-series computed with the numerical model was done using T\_TIDE (Pawlowicz et al., 2002). This provided a set of amplitude and phase values related to dominant astronomic constituents that were used to estimate currents at the Alcatraz monitoring site.

## 4. Results

### 4.1. Measurements

#### 4.1.1. Lateral transects

Volumetric rates of water and sediment flux for each of the 25 tracks along the outer and inner transects are summarized in Table 4. As a comparison to a previous study in June 1992 focusing on the transport of dredge material (Teeter et al., 1996), a piece-wise linear regression was fit to the data (Fig. 7). A linear fit through the flood- and most of the ebb-directed transports resulted in a slope of 0.033 and 0.013 for the January 2008 and June 1992 study periods, respectively. Of note is the difference in the cut-off position and slope for the fit of the strongly ebb directed flows. Teeter et al. observed a break in the data at ebbing flows of  $50\text{ k m}^3/\text{s}$  while the data collected as part of this study (January 2008) is only supported

Table 3  
Cohesive sediment parameters.

Parameter	Mud-2	Mud-4
Erosion parameter ( $M$ , $\text{kg}/\text{m}^2/\text{s}$ )	$5.5\text{E}-5$	$1.3\text{E}-5$
Settling velocity ( $w$ , $\text{mm}/\text{s}$ )	$3.0\text{E}-1$	$1.0\text{E}-1$
Critical bed shear stress for erosion ( $\tau_{cre}$ , $\text{N}/\text{m}^2$ )	$5.0\text{E}-1$	$1.35\text{E}-1$

by three points and shows that ebb flows in excess of  $120\text{ k m}^3/\text{s}$  yield a change in the sediment flux rate. The difference might be due to sampling protocol, measurement errors, availability of sediment, and variations in volumetric water flux between the two sampling periods. Measurements at the Fort Point tide gauge indicated that the tide range was 30 cm greater during the January 2008 study compared to the June 1992 Teeter et al. (1996) study.

The range of flux rates along both the inner and outer transects (Table 4) varied substantially and highlights the importance of integrating flux rates over full tide cycles. Such intense field campaigns are rarely practical and as such the use of numerical modeling, as was done for this study, offers an approach to filling in time and spatial gaps.

Two transects were chosen to illustrate the distributions of velocities along the inner transect during flood and ebb tides. Two measurements were made during spring tide that had large and comparable ebb and flood water and sediment fluxes, the first and fourth inner transects on Jan 24 (17:44 and 23:05, see Table 4). Water flux was  $\sim 90,000\text{ m}^3/\text{s}$  and sediment flux was  $\sim 3000\text{ kg}/\text{s}$  for both transects; the first transect was in the flood direction and the fourth transect was ebb directed. Fig. 8 shows the along channel and across channel velocity contours for the two transects. The east–north velocity vectors were rotated about the transect axis which was  $\sim 140^\circ$  from due east, to obtain along and across channel values. Distances across the channel are from the south bank. The along and across channel flood velocities (Fig. 8 right panels) illustrate what might be the formation of lateral eddies along both channel banks during flood tide. Along-channel flood contours contain regions of positive (ebb directed) flow at both channel margins. Also, across channel flood contours indicate flow toward the north bank (red contours) in the north part of the channel and flow toward the south in the south part of the channel. Ebb tide flow structures (Fig. 8, left panels) are substantially different from flood tide, with along channel velocities being positive and out of the Gate throughout the cross section. Also, across channel velocities illustrate topographic steering effects as flow approaches the Golden Gate constriction, i.e. velocities in the north part of the channel are directed toward the south and velocities in the south part of the channel are directed toward the north. These ebb and flood flow structures are also present in the numerical modeling results presented below.

#### 4.1.2. Point measurements (profiles)

Spring tide flood measurements revealed mid to upper water column velocities that ranged from still water to  $164\text{ cm}/\text{s}$  (Tables 2A and 2B). Flood directed velocities were never measured at the northern-most station, IT1, and only in the upper water column of IT6. These ‘outlier’ measurements are likely an artifact of the sampling locations.

SSC concentrations and median grain sizes ( $gs$ ) from the LISST (rmse  $7.1\text{ mg}/\text{L}$ ) exhibited variability both laterally across the channel and vertically with depth. Fig. 9 presents the lateral distribution of depth-averaged SSC for profile measurements that were made immediately following the ebb and flood transects described above and presented in Fig. 8 (both during spring tide). Ebb tide SSC was greatest at the southern-most station and decreased across the channel to the north. Flood tide SSC was more evenly distributed, with the lowest SSC in the middle of the channel and the higher SSC near both banks. Median grain sizes exhibited minimal lateral variability during both ebb and flood tides, with all stations within  $\sim 10\%$  of the mean. Also, the mean grain size was comparable during ebb and flood tide ( $\sim 40\text{ }\mu\text{m}$ ).

Fig. 10 shows the vertical distribution of laterally-averaged SSC and median grain size for the same ebb and flood tides as Figs. 8 and 9. For each tide, data from all seven stations were averaged to obtain the laterally-averaged values. SSC tended to be greatest near the bed and decrease toward the surface (Fig. 10, top panels). SSC profiles

**Table 4**  
Measured water and sediment flux rates across the Golden Gate.<sup>a</sup>

Transect	Start time (UTC)	End time (UTC)	Start tide (m)	Water flux (m <sup>3</sup> /s)	Sediment flux (kg/s)	
<i>Neap tide</i>						
Outer	1/16/08 14:41	1/16/08 15:28	0.382	59,800	1800	
	1/16/08 16:47	1/16/08 17:18	0.80	122,200	4000	
	1/16/08 18:43	1/16/08 19:14	1.00	87,100	2800	
	1/16/08 20:30	1/16/08 21:11	0.93	20,400	730	
	1/16/08 23:06	1/16/08 23:46	0.70	(67,700)	(2000)	
	1/17/08 2:05	1/17/08 2:39	1.10	(50,900)	(1600)	
	1/17/08 2:44	1/17/08 3:18	1.27	(28,800)	(920)	
Ebb range				20,400–122,200	730–4000	
Flood range				(28,800)–(67,700)	(920)–(2000)	
Inner	1/17/08 16:06	1/17/08 16:34	0.32	69,100	2000	
	1/17/08 18:09	1/17/08 18:31	0.84	97,400	3100	
	1/17/08 19:47	1/17/08 20:07	1.09	87,100	2800	
	1/17/08 21:31	1/17/08 21:56	1.09	33,800	1100	
	1/17/08 23:25	1/17/08 23:50	0.90	(24,800)	(990)	
Ebb range				33,800–97,400	1100–3100	
Flood range				(24,800)	(990)	
<i>Spring tide</i>						
Outer	1/23/08 15:21	1/23/08 16:01	0.53	(62,300)	(2300)	
	1/23/08 16:55	1/23/08 17:28	−0.11	(107,300)	(3600)	
	1/23/08 18:41	1/23/08 19:15	−0.31	(80,800)	(2600)	
	1/23/08 20:32	1/23/08 21:10	0.18	26,400	890	
	1/23/08 22:15	1/23/08 22:44	0.90	122,700	4800	
	1/23/08 23:52	1/24/08 0:50	1.44	128,500	6200	
	1/24/08 1:30	1/24/08 2:19	1.67	84,800	3300	
	1/24/08 3:16	1/24/08 3:45	1.37	13,900	560	
	Ebb range				13,900–128,500	560–6200
	Flood range				(62,300)–(107,300)	(2300)–(3600)
Inner	1/24/08 17:44	1/24/08 18:06	0.07	(89,100)	(3000)	
	1/24/08 19:54	1/24/08 20:08	0.06	(59,400)	(1800)	
	1/24/08 21:15	1/24/08 21:35	0.45	5000	240	
	1/24/08 23:05	1/24/08 23:22	1.15	93,500	3100	
	1/25/08 1:23	1/25/08 1:39	1.73	83,600	3100	
Ebb range				5000–93,500	240–3100	
Flood range				(59,400)–(89,100)	(1800)–(3000)	

<sup>a</sup> Negative (flood) values shown in parenthesis.

were very similar during ebb and flood tide conditions. Median grain sizes showed little variability with depth, similar to the lateral distributions. Again, median grain sizes were comparable between ebb and flood tide and varied little from the mean value of ~40  $\mu\text{m}$ .

## 4.2. Model simulations

### 4.2.1. Comparison of modeled and measured water and sediment flux

Measured and modeled cross-sectional averaged volumetric water flux compare very well ( $r^2 = 0.98$ , Fig. 11A; see also Elias and Hansen, 2012 for further comparison). Employing optimized

sediment calibration parameters (Table 3), the sediment mass flux rates also compare well with measurements and explain ~93% of the variance (Fig. 11B). The greatest discrepancy is at peak spring tide along the outer transect where the model over-estimates net outward flux. Only simulation results from the inner transect were used for development of the relationship between Alcatraz SSC and flux at the Gate in this study.

Cross channel observations in Fig. 8 were depth-averaged and compared to model simulated currents in the along and cross channel directions for ebb and flood tides (Fig. 12). The change in current direction across the channel is evident in both the observed and

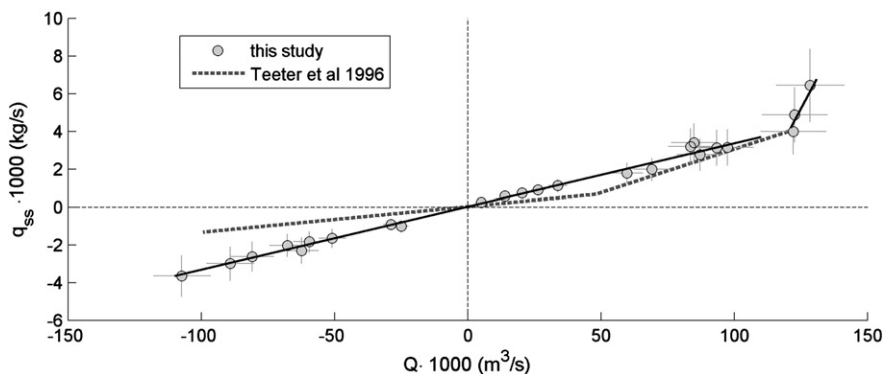


**Fig. 7.** Measured mass sediment and volumetric water flux across Golden Gate as measured in this study and by Teeter et al. (1996). Piecewise linear regressions for ebb and flood are shown with the solid line for the data collected in 2008. Cross-hairs denote 10% and 30% uncertainty in volumetric water flux ( $Q$ ) and mass sediment flux ( $q_{ss}$ ) measurements, respectively.

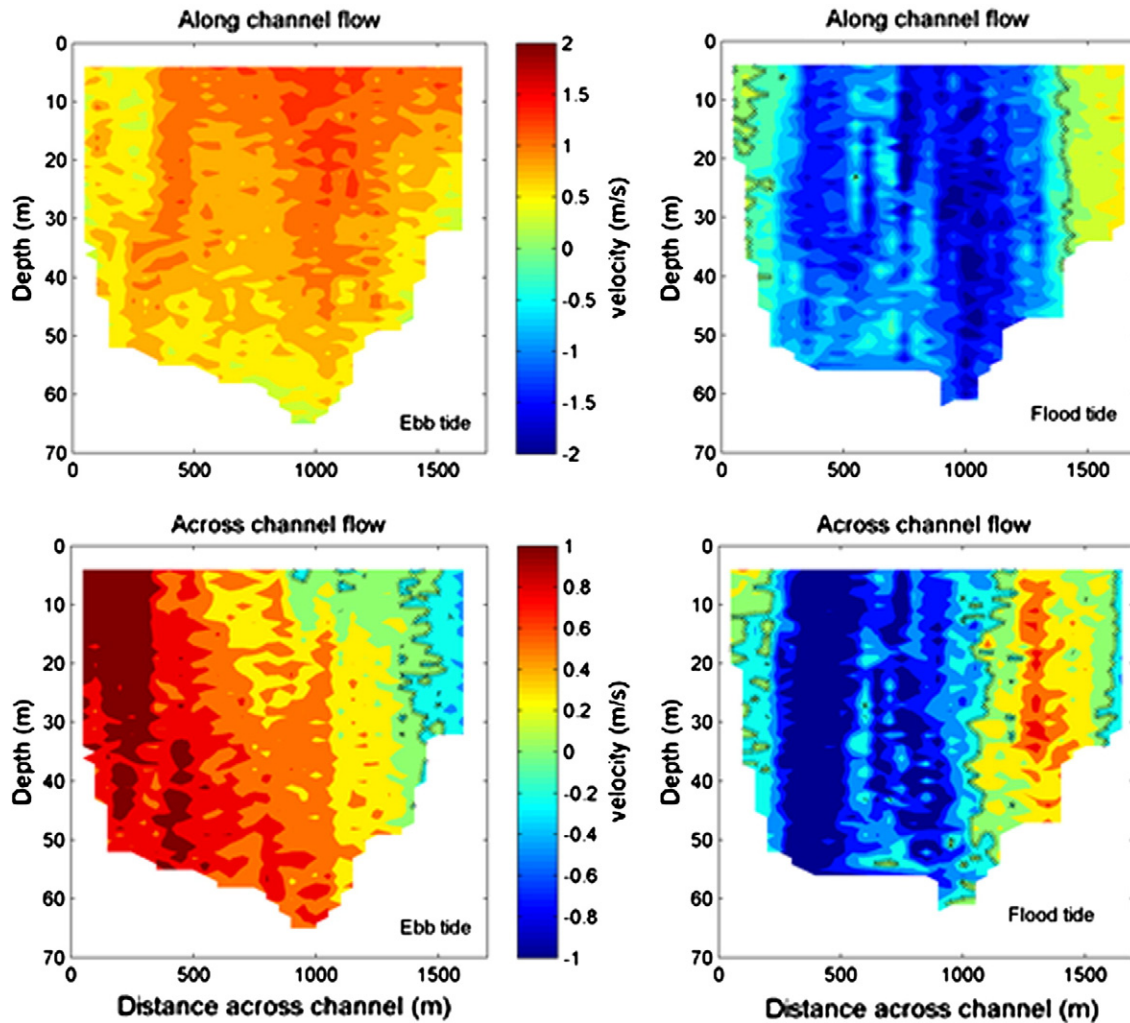


**Fig. 8.** Contours of along channel (top) and across channel (bottom) velocities (m/s) for ebb (left) and flood (right) tides. Transects shown are from Jan 24, 17:44 (flood) and 23:05 (ebb), see Table 3. Black dashed lines are the zero velocity contours. Along channel, positive values (red) denote ebb direction and negative values (blue) denote flood direction. Across channel, positive values (red) denote flow toward the north and negative values (blue) denote flow toward the south. Note the difference in color scale between the along channel (top) and across channel (bottom) panels.

simulated results, particularly for the cross channel ebb tide case (Fig. 12A). The flow reversal was not as apparent in the model results for the flood event shown in Fig. 12, but was present at other times.

#### 4.2.2. Tidally-varying eddies affecting sediment transport patterns

Model-simulated sediment transport patterns for various stages of the tide illustrate the spatial variation in transport rates across the Golden Gate inlet (Fig. 13). There is significant lateral variability in the instantaneous flux across the inlet; an observation noted by Fram et al. (2007), Fram (2005) and Martin et al. (2007) based on measurements and analysis of chlorophyll and salt flux through the Golden Gate. Fram (2005) and Fram et al. (2007) showed the presence of a tidally trapped counter-clockwise eddy that forms during the second half of the flood tide between Point Cavallo and Angel Island. As the tide decelerates, the eddy moves out into the channel near the end of flood tide. These patterns are also evident in model simulations conducted for this study (Fig. 13B and C). In addition to the tidally trapped eddy east of Point Cavallo, the model also indicates the formation of eddies landward (east of) of Fort Point and the point across the Golden Gate at the south and north terminus of transect IT (Fig. 13A and B) during the flood tide. During ebb tide, the pattern is translated to the seaward side of the Points such that a counter-clockwise eddy forms at Baker Beach west of Ft. Point and smaller clockwise eddy at Bonita Cove at the north end of the channel

(Fig. 13D; Fig. 8, Elias and Hansen, 2012). From this it can be seen that neither point measurements nor short term flux estimates are sufficient to accurately describe the net flux at Golden Gate which is subject to strong tidal currents, diurnal asymmetry, and complex bathymetry. Furthermore, instantaneous flux (Fig. 13F) is orders of magnitude greater than the net flux (as shown later), and requires integration with respect to both time and space in order to obtain an accurate estimate of the total net flux.

### 4.3. SSC monitoring as a proxy to Golden Gate suspended sediment flux

#### 4.3.1. SSC at the Alcatraz monitoring site

Instantaneous SSC at Alcatraz is strongly modulated by tides and to some degree, sediment flux into San Francisco Bay via the Delta. The periodic signal of the Alcatraz SSC time-series suggests variations in concert with semi-diurnal and spring-neap tide cycles (Fig. 14A). A power spectral density estimate of SSC measured at Alcatraz (155 days,  $f = 0.001$  Hz, Welch, NFFT = 1024) yields peaks at 10.8 days, 25.8 h, and 12.3 h, similar to peak frequencies of tide-induced water levels at the nearby San Francisco tide gauge (dominant peaks at 21.3 days, 23.81 h, and 12.49 h). The peaks at 12.3 and 25.8 h are related to the dominant tide signal,  $M_2$  ( $f = 0.0805$  h<sup>-1</sup>) while the 10.8 day periodicity reflects the spring-neap cycles. Highest SSCs at Alcatraz were measured in early to mid-January (Fig. 14A and

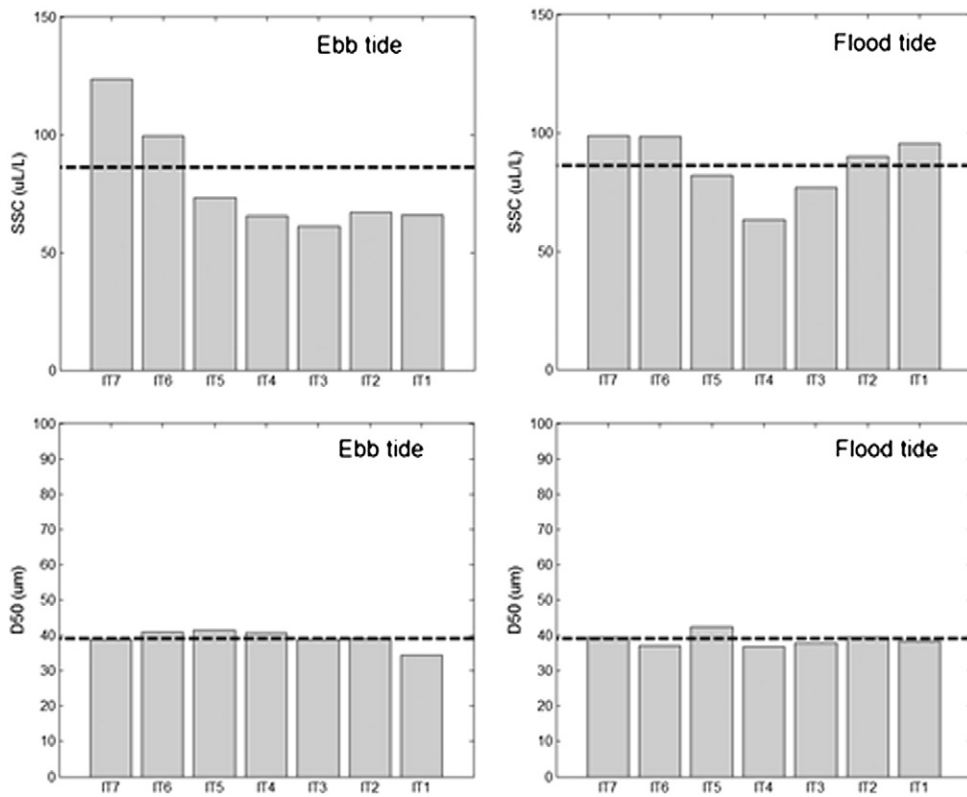


**Fig. 9.** Lateral distributions of depth-average SSC and median grain size for ebb and flood tides. Measurements were made immediately following the transects shown in Fig. 8. Black dashed lines indicate the mean values for the data in each panel.

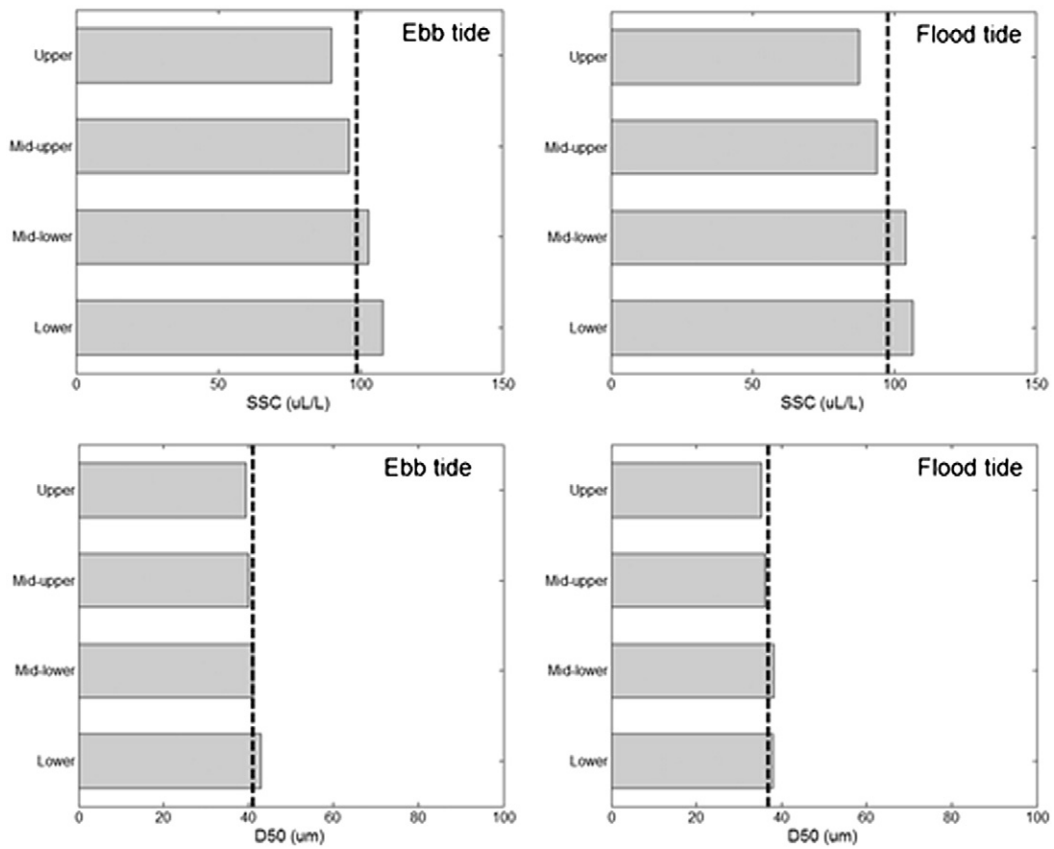


**Fig. 10.** Vertical distributions of laterally-averaged SSC and median grain sizes for ebb and flood tides. Measurements were made immediately following the transects shown in Fig. 8. Black dashed lines indicate the mean values for the data in each panel.

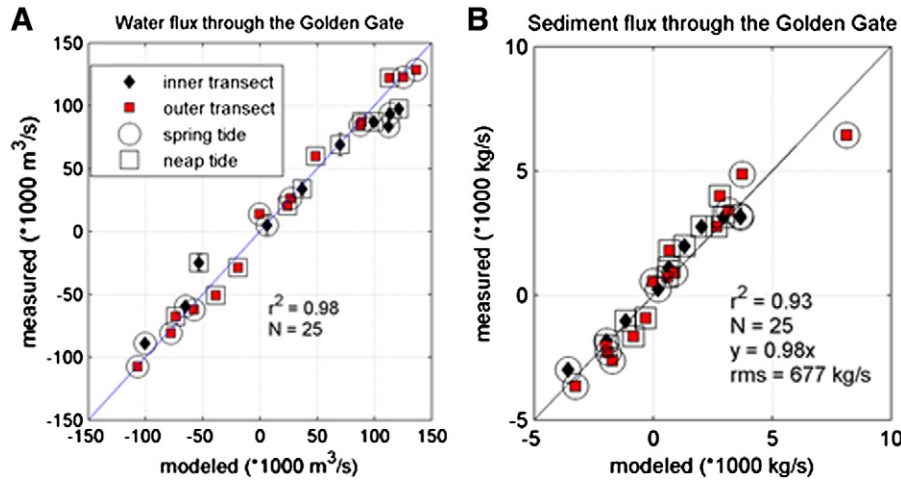


**Fig. 11.** Comparison of modeled and measured (A) water discharge and (B) suspended flux through the Golden Gate. Solid line in (A) depicts perfect fit; solid line in (B) depicts best fit linear line with zero y-intercept.

C) and coincided with the highest tides of the year (perigee lunar alignment). Concentrations are highest during the transition from ebb to flood of the lower low stage of the tide (Fig. 14C).

Upon initial inspection of the time-series SSC data, a clear dependence of Alcatraz sediment concentrations to measured SSC at the Mallard Island monitoring site is not evident. A more direct comparison of sediment loads with Alcatraz SSCs elucidates the relationship. The daily advective sediment load from the Delta was estimated with the product of daily averaged Mallard Island SSCs and Delta freshwater inflows from the Dayflow model. The load estimate may be somewhat of an over-estimate as the landward dispersive load was not accounted for, which might reduce the amount by ~20% of the total (McKee et al., 2006), but overall the estimate should be reasonable. Cross-correlations indicate a delay of 8 days or more in the response of the Alcatraz SSC measurements to sediment loading from the Delta. A 12 day lag of the Alcatraz SSC data suggests a linear trend with sediment loadings <3000 t/day (Fig. 14D), while at greater loading rates the sediment plume appears to migrate down-estuary somewhat quicker (8 day lag; inset Fig. 14D). Although the correlations between sediment loading and SSC measurements at Alcatraz are weak ( $r^2 = 0.14$  for loadings <3000 t/day and  $r^2 < 0.1$  for higher loading rates), visual inspection of the lower bounds indicate an increase in daily averaged SSC at Alcatraz in response to increased sediment loads at Mallard Island. The low correlations, which represent a linear least square fit through all the data, are likely due to the unusually low sediment influx to the system during WY08 and concealment of the signal at Alcatraz by SSC from other sources and processes that are of equal or greater magnitude. It is expected that similar analysis of data from

'normal' water years would show a greater dependence of SSC at Alcatraz to advective sediment loads from the upper reaches of North Bay.

#### 4.3.2. Currents at the Alcatraz monitoring site

The tidal ellipse of numerically modeled currents at Alcatraz was bi-directional with an ebb preference (Fig. 15A). Harmonic analyses indicate that east- and north-directed velocities can be well represented with six tidal constituents (Table 5). Re-construction of the tidal currents for the time-period spanning January 01–April 30 2008, using T\_TIDE and the tidal amplitudes and phases listed in Table 5 resulted in *rms* errors = 0.11 m/s and 0.12 m/s for the east- and north-directed currents, respectively (Fig. 15B).

A time-series of current magnitudes computed with the numerical model is plotted in Fig. 16A. A positive or negative value was assigned for ebb or flood, respectively, based on the orientation of the tidal ellipse defined in Fig. 15A. The low-pass filtered (tide-averaged) signal is shown with the solid black line and is mostly positive illustrating the net ebb directed flow. The low-pass filtered signal is repeated in Fig. 16B and compared to the time-series reconstructed from tidal constituents. The reconstructed time-series compares well with the full low-pass filtered signal, and forms the basis for computing advective and dispersive flows at Alcatraz that are used in the development of the relationship linking surrogate measurements at Alcatraz with suspended sediment flux at the Gate.

#### 4.3.3. Sediment flux at the Golden Gate

In developing an analytical relationship whereby measurements can be used to estimate the net sediment flux at the Golden Gate,

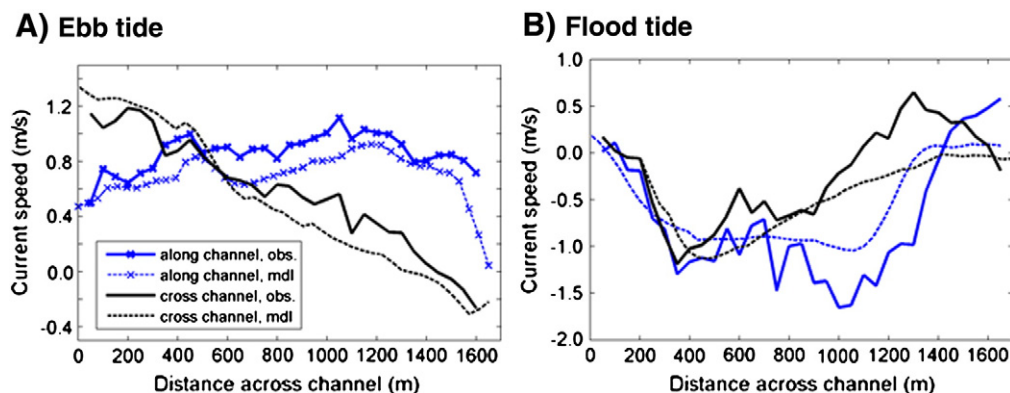


**Fig. 12.** Comparison of modeled and measured depth-averaged velocities across the channel for (A) ebb and (B) flood conditions shown in Fig. 8.

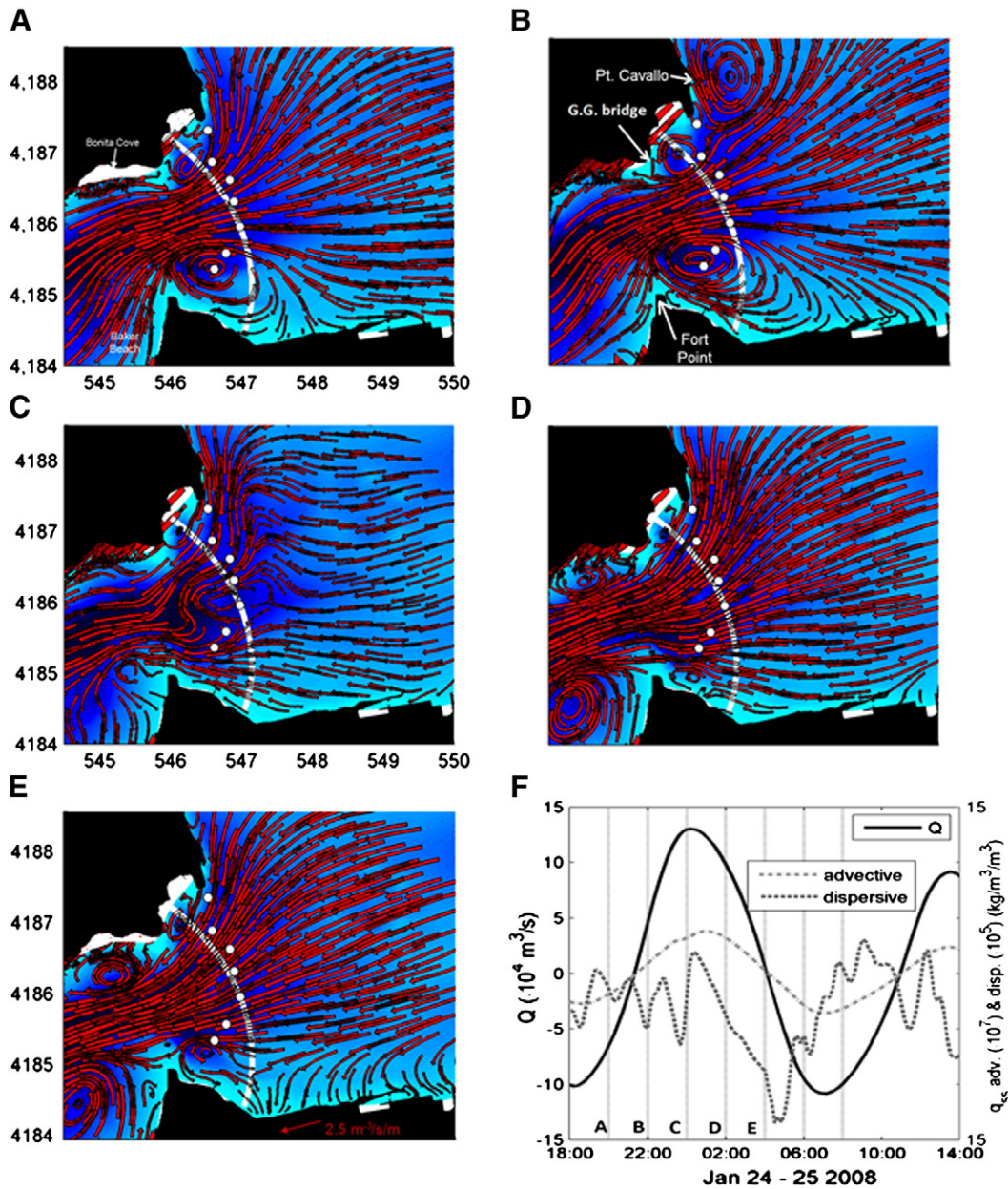


**Fig. 13.** Modeled sediment transport streamlines during various stages of the tide. Tidal stage is illustrated in subplot (F) with vertical dashed lines. Instantaneous volumetric water and mass advective and dispersive sediment flux are shown with the curved lines. The scale for dispersive flux is 100 times smaller than that for advective flux so its variability can be seen on the graph.

the two primary flux terms (advective and dispersive) in Eq. (1) were computed with Alcatraz observation data and plotted against tide-averaged total suspended sediment flux at the Golden Gate (January through April 2008) for tide-averaging periods of 20 h, 25 h, 30 h, and 35 h. While three of four tide-averaging periods for the dispersion term (Eq. (1), term 2) were statistically significant, coefficients of determination ( $r^2$ ) were all less than 0.05 (Table 6). The advection term was statistically significant ( $p$ -value  $< 0.05$ ) for all tide-averaging periods tested and yielded  $r^2$  values ranging from 0.52 (35 h tide-averaging) to 0.86 (25 h tide-averaging). Instantaneous and 25 h tide-averaged sediment flux at the Golden Gate are shown in Fig. 17.

A scatter plot of low-pass filtered (25 h) suspended sediment flux at the Golden Gate compares well with the low-pass filtered Alcatraz advective term ( $[SSC][U]$ , Fig. 18). Least-squares fits between the data yielded a linear and second order polynomial relationship of about

equal goodness-of-fit ( $r^2 = 0.86$ ,  $rmse = 67.2$  kg/s and  $r^2 = 0.87$ ,  $rmse = 66.3$  kg/s, respectively). As the second-order polynomial is only marginally better, we have chosen to employ the linear fit describing flux at the Gate with SSC,

$$F_{GG} = 1.21 \cdot 10^5 \cdot [SSC] \cdot [U] + 40.3 \quad (2)$$

where  $F_{GG}$  (kg/s) is the 25 h low-pass (tide-averaged) filtered suspended sediment flux at the Golden Gate,  $[SSC]$  is the measured tide-averaged suspended sediment concentration at the Alcatraz monitoring site ( $\text{kg}/\text{m}^3$ ), and  $[U]$  the tide-averaged currents (m/s) computed from tidal constituents in Table 5.

Application of Eq. (2) with Alcatraz SSC data for water years 2004 through 2010 resulted in predominantly seaward directed sediment flux (Fig. 19). Net 25 h averaged flux rates were typically  $< 800$  kg/s but reached nearly 1500 kg/s in early 2006 coincident with high

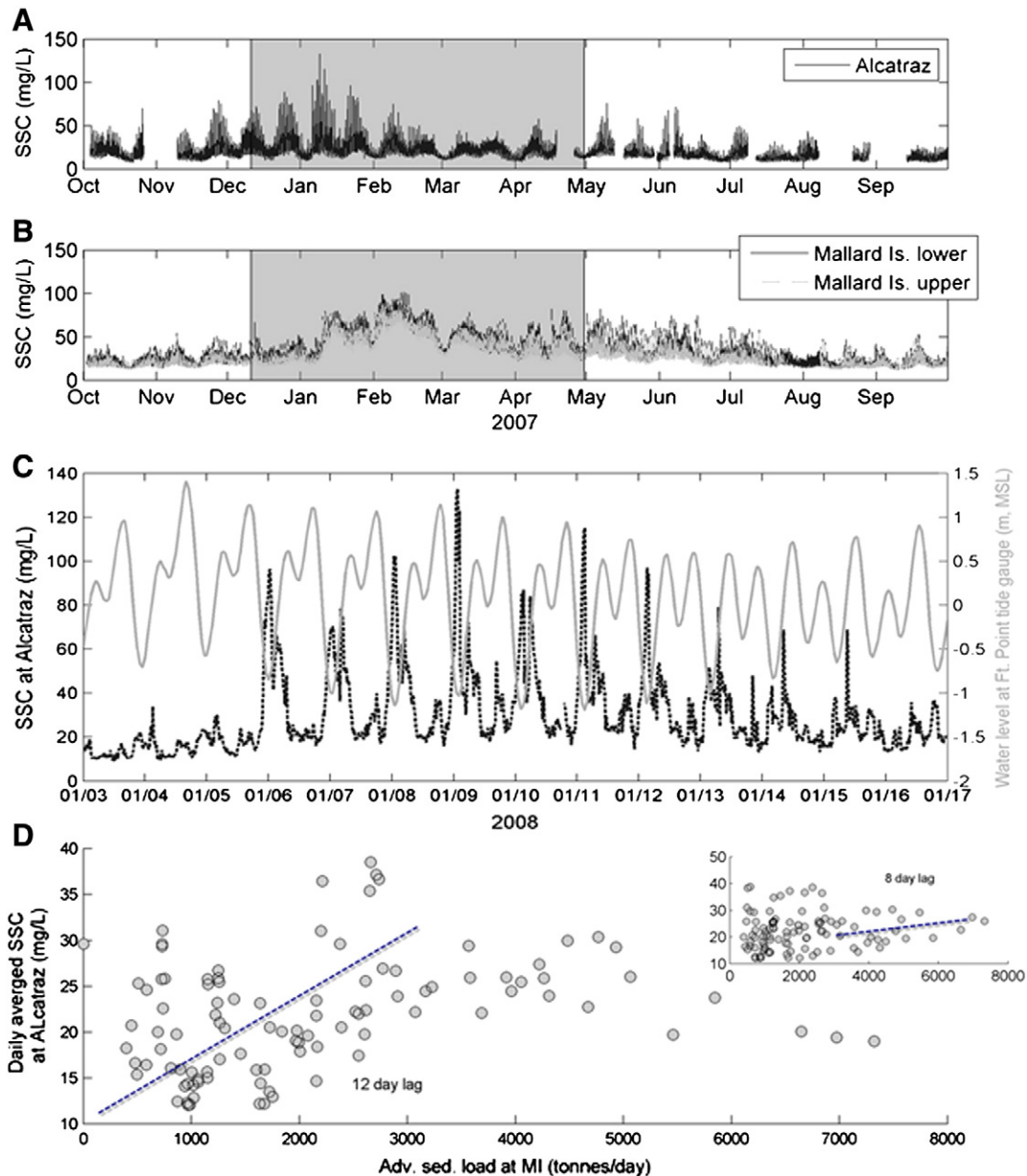


**Fig. 14.** Suspended sediment concentrations at Alcatraz and its relation to the tide regime and sediment load from the Delta. (A and B) Instantaneous suspended sediment concentration (SSC) for water year 2007 (October 01, 2007 through September 30, 2008) at Alcatraz and Mallard Island. Gray shaded areas denote time-period simulated with the numerical model. December to January simulation results excluded from analyses as this time-period was used for 'model spin-up'. (C) Tide-averaged SSC at Alcatraz shows a relatively strong correlation with the tide-range measured at the nearby Ft. Point San Francisco tide station. (D) Instantaneous measured SSC at Alcatraz and water level at the tide station illustrates the coincidence of a higher tide range and low water levels with elevated SSCs. (E) Daily averaged SSC at Alcatraz plotted against the inferred sediment load from the Delta at Mallard Island (January through April 2008).

Delta flows. Total net annual flux ranged from 1.1 Mt (million metric tons) to 1.3 Mt with a mean rate of 1.2 Mt. The highest rate was in WY2006 and coincided with the peak and high Delta flows in January 2006 (Fig. 19). Tide periods with incomplete SSC data were filled in with mean values representative of each water year. Water year 2010 had the lowest number of complete tide-cycles with nearly half missing.

## 5. Discussion

The study period, determined by the timing of the sediment flux measurements at the Golden Gate obtained as part of this study, happened to coincide with a critically dry water year. Using satellite images from 1995, Ruhl et al. (2001) showed that sediment plumes

can extend from the Delta to >10 km seaward of the Golden Gate during high Delta inflows, while during low flows ( $\sim 1700 \text{ m}^3/\text{s}$ ), a plume is barely discernible south of San Pablo. The maximum Delta flow rate achieved during the WY08 study period was  $1500 \text{ m}^3/\text{s}$  and comparable to the low flows of the satellite imagery. The relatively insignificant contribution of point source sediment exchange at the Golden Gate calculated with the model and weak correlation between the point source load and measured SSC at Alcatraz is thus not surprising. A question that remains is if the predictor equation (Eq. (2)), developed under conditions of very low flow and sediment loading conditions, is valid for higher freshwater flows and sediment loads. Two primary questions need to be addressed in order for the relationship to hold: 1) do Alcatraz SSC measurements sufficiently reflect the total sediment load available for exchange at the Golden Gate

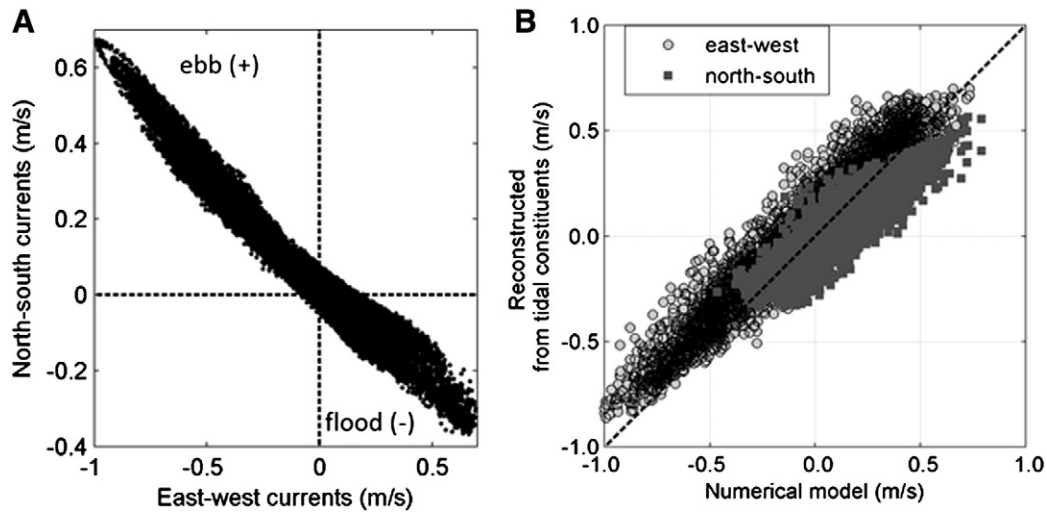


**Fig. 15.** Modeled hourly depth-averaged currents at Alcatraz. (A) Tidal ellipse at the Alcatraz monitoring site is oriented in the northwest/southeast direction. Ebb is defined as positive. (B) Reconstructed currents calculated with tidal constituents listed in Table 5 plotted against numerically modeled currents at Alcatraz. Dashed line depicts perfect fit.

(from all sources within the Bay), and 2) does the relationship sufficiently account for changes in flow regime in response to high freshwater loadings?

Comparison of the SSC record at Alcatraz (calendar years 2004 to 2010) with Delta flows shows that SSC measurements do reflect inputs from the Delta at high flow rates (Fig. 20). Least-squares linear fits of all available tide-averaged data yields  $r^2 = 0.17$  ( $N = 1416$ ). At higher Delta flow rates  $> 3000 \text{ m}^3/\text{s}$ , the SSC response is substantially more evident ( $r^2 = 0.42$ ; inset of Fig. 20). The seemingly random SSC values below  $50 \text{ mg/L}$  does include the signal from the Delta as shown previously, but is masked by re-suspended material, sediment that is kept in suspension and transported due to persistent tidal and other currents, and loadings from other sources at the boundaries of the Bay (e.g., tributaries and open ocean boundary). Because the Alcatraz monitoring site is located in Central Bay at the confluence of both the northern and southern reaches of San Francisco Bay, elevated SSC values that correlate well with Delta flows above the  $3000 \text{ m}^3/\text{s}$  threshold likely also reflect loadings from other tributaries that supply sediment during times of high precipitation events. This can be important as the sediment yield from the Delta decreases in response to the ceased 19th Century hydraulic mining era and the relative contribution of sediment supply from other sources increases (McKee et al., 2013–this issue). Linkages between other sediment sources and measured SSCs at Alcatraz have not yet been investigated but would provide useful information for the assessment of utilizing the Alcatraz monitoring site as a proxy to flux from other sources through the Gate in the future.

With respect to the second issue regarding representation of freshwater exchange, it is pointed out that details of the flow dynamics are not necessary but rather, the gross behavior and overall net volumetric water flux per tide cycle is required (sediment is assumed to be represented by measured SSC and calibration constants).

Gravitational circulation and baroclinic flows, which become increasingly important with higher freshwater loadings, were not fully accounted for in this study as freshwater inputs were minimal and the model was implemented in a vertically averaged mode. Parameterization of changes in the flow dynamics and net flux rates could be developed with a 3D numerical model and high freshwater point source loadings. With the current state of knowledge, it is uncertain if such parameterization would result in the necessity to adjust Eq. (2).

We estimate that the mean suspended-sediment outflow from San Francisco Bay during WY2004–2010 was  $1.2 \text{ Mt/yr}$  which is less than a previous estimate of  $5.0 \text{ Mt/yr}$  during 1955–1990 developed from bathymetric surveys and conservation of mass (Schoellhamer et al., 2005). This early estimate is larger likely because it included bed load, higher freshwater flows than experienced in WY2004–2010, and it was for a period prior to a 36% step decrease in Bay SSC in 1999 that may indicate that the Bay crossed a threshold from transport to supply regulation of sediment transport (Schoellhamer, 2011).

Watershed disturbances increased sediment supply to San Francisco Bay in the 19th and early 20th centuries and since then the Bay has been geomorphically adjusting to a decreasing sediment supply (Schoellhamer et al., 2013–this issue). Schoellhamer et al. (2013–this issue) hypothesize that San Francisco Bay is still capable of adjusting but further adjustment will occur only during greater floods than previously experienced during the adjustment period. Periods of equilibrium are likely between these adjustment floods. The mean sediment outflow from San Francisco Bay during WY2004–2010 was  $1.2 \text{ Mt/yr}$  which is similar to the mean sediment inflow of  $1.4 \pm 0.5 \text{ Mt/yr}$  for the same period reported by McKee et al. (2013–this issue, Table 5). Thus, during the study period, San Francisco Bay sediment inflow and outflow were roughly in balance.

**Table 5**

Tidal constituent amplitudes and phases for estimation of currents at the Alcatraz monitoring site.

Tidal constituent	Frequency ( $\text{h}^{-1}$ )	East-directed amplitude	East-directed phase	North-directed amplitude	North-directed phase
M2	0.0805	0.49	142.94	0.26	321.14
S2	0.0833	0.14	148.19	0.07	329.77
N2	0.0790	0.11	125.19	0.06	308.28
K1	0.0418	0.11	140.88	0.06	322.51
O1	0.0387	0.08	135.68	0.05	321.70
Q1	0.0372	0.02	134.97	0.01	315.90

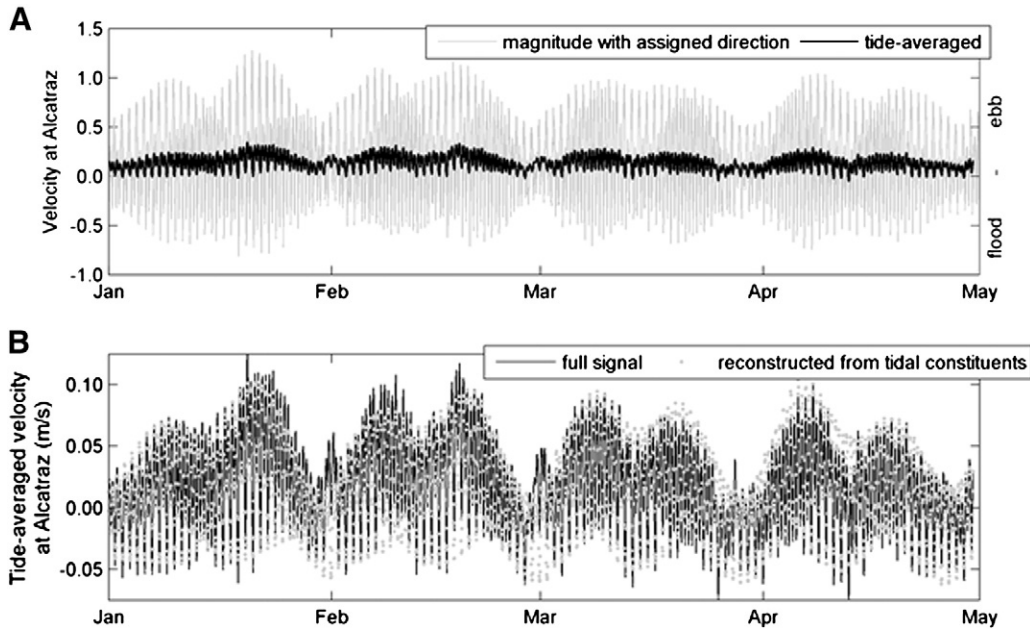


**Fig. 16.** Currents at the Alcatraz monitoring site. (A) Current magnitudes with assigned negative values for flood directed flows (based on tidal ellipse in Fig. 15A) and the 25 h low-pass filtered signal. (B) Comparison of the low-pass filtered time-series from the full current signal in (A) and the tide-averaged signal of currents reconstructed with tidal constituents in Table 5.

**Table 6**

Coefficients of determination ( $r^2$ ) of advective and dispersive sediment flux terms with total flux at the Golden Gate using different tide-averaging periods.

Term	20 h tide avg.	25 h tide avg.	30 h tide avg.	35 h tide avg.
Advective	0.83	<b>0.86</b>	0.78	0.52
Dispersive	NS	0.00	0.00	0.04

NS: not statistically significant ( $p$ -value > 0.05). Bold value indicates highest value obtained.

No large floods occurred during the study period, so this result is consistent with the adjustment hypothesis.

**6. Conclusions**

In an effort to reduce the uncertainty of the least well characterized component of the San Francisco Bay sediment budget, an equation relating SSC measurements at the Alcatraz monitoring site with tide-averaged suspended sediment fluxes through the Golden Gate was developed. The relation was developed from suspended

sediment flux rates computed with a numerical model; the model was calibrated against measurements obtained across the Golden Gate over a spring–neap tide cycle. Observed suspended sediment concentrations (SSC) from the Alcatraz monitoring station were then used to parameterize advective and dispersive fluxes and plotted against five months of hind-cast sediment flux rates at the Golden Gate.

Measurements and model simulations indicated horizontal spatial gradients of both water and sediment flux across the Golden Gate. Some of this can be attributed to the formation of eddies on both sides of the landmass points at the constriction of the Gate. At flood tide, two large counter-clockwise and one clockwise eddy forms landward of the Gate; at ebb tide, at least one of each clockwise and counter-clockwise eddy forms on the seaward side of the Gate. Depth-averaged suspended sediment concentrations showed variation across the channel; at ebb tide there was a decrease from south to north, while at flood tide, the concentrations were about equal along the channel banks and lower in the center of the channel. The rather complex flow and transport patterns observed in the measurements and elucidated with the model illustrate the added value of

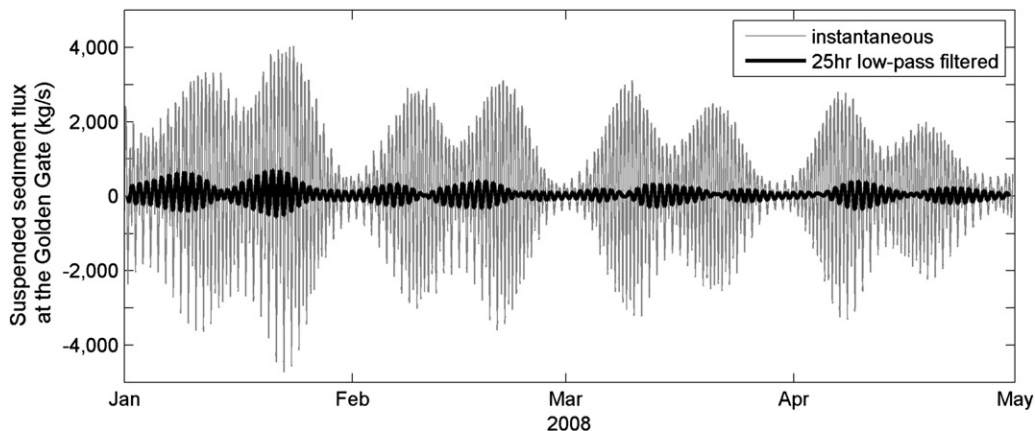


**Fig. 17.** Modeled suspended sediment flux across the inner transect of the Golden Gate from January through April 2008. 25 h low-pass filtered (tide-averaged) values are shown with bold line and plotted against the right axis. Positive values indicate seaward flux.

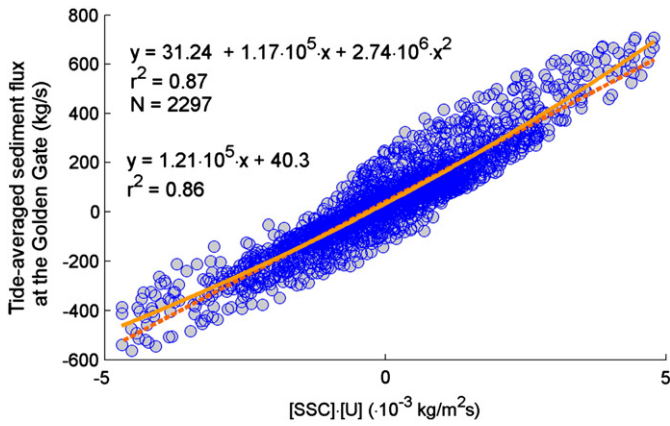


Fig. 18. Low-pass filtered (25 h) sediment flux rates at the Golden Gate versus measured SSC and computed currents at the Alcatraz monitoring site. Positive flux is seaward.

employing a numerical model to capture the net sediment flux at this site.

Suspended sediment concentrations measured at the Alcatraz monitoring station were shown to be modulated by tides and sediment loading from the Sacramento–San Joaquin Delta. Maximum tidal currents coincided with the latter part of the lower low ebb cycle at the Alcatraz monitoring site and were largely responsible for the higher SSC concentrations. The study period encompassed a critically dry water year and as a result, sediment loading rates from the Delta were unusually low. Although only weak correlations between observed SSCs at Alcatraz and model simulated flux through the Golden Gate with Delta loading rates were attained, both model simulation results and measurements indicated a sediment pulse transport rate of 8 to 12 days from Suisun to Central Bay.

A linear fit relating the 25 h tide averaged product of computed currents and observed SSCs at Alcatraz with net sediment flux through the Golden Gate was developed. Utilization of the equation with all available Alcatraz SSC data resulted in a mean sediment outflow for WY2004–2010 of 1.2 Mt/yr. This value is roughly equivalent to independently calculated sediment inflow during the study period ( $1.4 \text{ Mt} \pm 0.5$ , McKee et al., 2013–this issue). While there was little variation in sediment outflow from year to year, exports were computed to be greatest during the wettest water year (WY2006) analyzed but only marginally so.

**Acknowledgments**

We extend our gratitude to Megan Sheridan and Chris Halle at Bodega Marine Lab, Bodega, CA who collected and post-processed a significant portion of the data and Paul Buchanan who manually collected the point suspended-sediment samples used for instrument calibration. Thanks also to two anonymous reviewers who provided constructive critiques of the manuscript. Financial support was provided by the USGS San Francisco Bay project (Principal Investigator Patrick Barnard).

**References**

Ariathurai, C., 1974. *A Finite Element Model for Sediment Transport in Estuaries*. (PhD Dissertation) UC Davis, Davis.  
 Barnard, P.L., Eshleman, J., Erikson, L., Hanes, D.M., 2007. *Coastal Processes Study at Ocean Beach, San Francisco, CA: Summary of Data Collection 2004–2006*. U.S. Geological Survey, Santa Cruz, CA.  
 Barnard, P., Hanes, D., Lescinski, J., Elias, E., 2007. *Monitoring and Modeling Nearshore Dredge Disposal for Indirect Beach Nourishment, Ocean Beach, San Francisco*. ASCE, San Diego 4192–4204.  
 Barnard, P., Erikson, L., Kvitek, R., 2011. *Small-scale sediment transport patterns and bedform morphodynamics: new insights from high resolution multibeam bathymetry*. *Geo-Marine Letters* 31 (4), 227–236.  
 Buchanan, P., Lionberger, M., 2006. *Summary of Suspended Sediment Concentration Data, San Francisco Bay, California, Water Year 2004*. U.S. Geological Survey. Data Series 226.

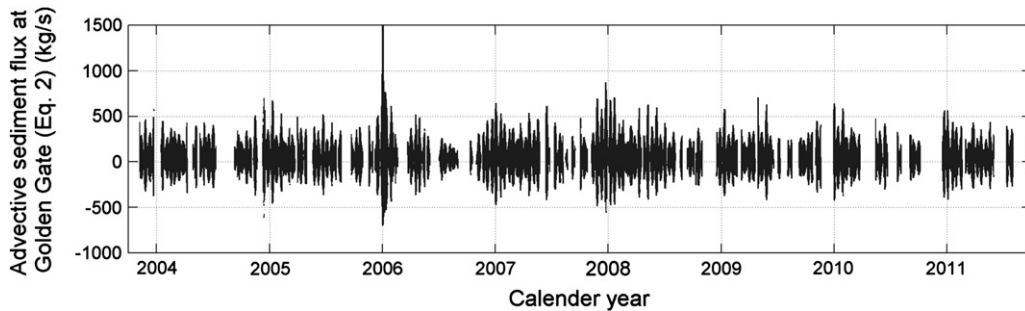


Fig. 19. Net tide averaged advective sediment flux at the Golden Gate calculated with the empirical fit, Eq. (2). Positive flux is directed seaward.

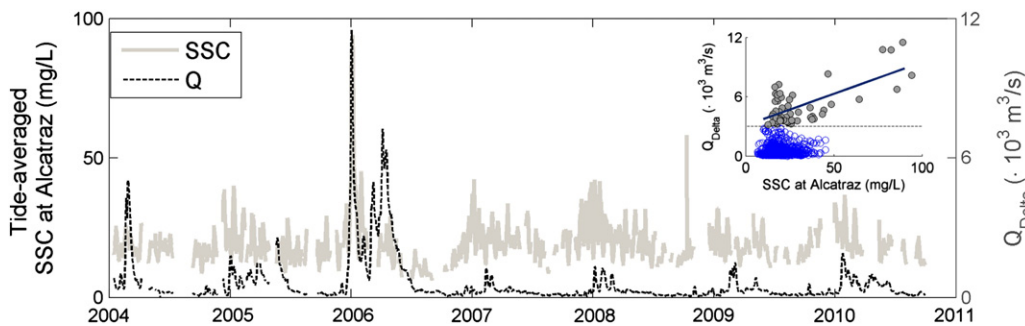


Fig. 20. Tide-averaged (30 h) SSC at Alcatraz and Delta inflows to the Bay. Inset shows the same data as a scatter plot with a least-squares linear regression ( $r^2 = 0.42$ ) through data above a threshold of  $Q_{Delta} = 3000 \text{ m}^3/\text{s}$ .

- Carlson, P., McCulloch, D., 1974. Aerial Observations of Suspended Sediment Plumes in San Francisco Bay and Adjacent Pacific Ocean. U.S. Geological Survey, s.l.
- CDWR, 2012. DAYFLOW program documentation and DAYFLOW data summary user's guide. Available at: <http://iep.water.ca.gov/dayflow> (Accessed 2012).
- Cheng, R., Smith, R., 1998. A Nowcast Model for Tides and Tidal Currents in San Francisco Bay, California. Marine Technology Society, Baltimore, MD 537–543.
- Chin, J., et al., 2010. Estuarine Sedimentation, Sediment Character, and Foraminiferal Distribution in Central San Francisco Bay, California. U.S. Geological Survey, s.l.
- Chin, J.L., Wong, F.L., Carlson, P.R., 2004. Shifting shoals and shattered rocks – how man has transformed the floor of west-central San Francisco Bay. U.S. Geological Survey Circular 1259.
- Conomos, T., 1979. Properties and Circulation of San Francisco Bay Water. Pacific Division of the American Association for the Advancement of Science, San Francisco 47–84.
- Conomos, T., Peterson, D., 1977. Suspended-particle transport and circulation in San Francisco Bay, an overview. Estuarine Processes. Academic Press, New York, pp. 82–97.
- Conomos, T., Smith, R., Gartner, J., 1985. Environmental setting of San Francisco Bay. *Hydrobiologia* 129 (1), 1–12.
- Deltares, 2011. User Manual Delft3D-FLOW. 3.15.18392.
- Dyer, K., 1997. Estuaries – Physical Introduction, 2nd ed. John Wiley and Sons, Chichester.
- Edwards, T.K., Glysson, G.D., 1999. Field methods for measurements of fluvial sediments. U.S. Geological Survey, Techniques of Water Resources Investigations, Book3, Chapter C2.
- Egbert, G., Erofeeva, S., 2002. Efficient inverse modeling of barotropic ocean tides. *Journal of Atmospheric and Oceanic Technology* 183–204.
- Egbert, G., Bennett, A., Foreman, M., 1994. TOPEX/POSEIDON tides estimated using a global inverse model. *Journal of Geophysical Research* 99 (C12), 821–824.
- Elias, E.P.L., Hansen, J.E., 2012. Understanding processes controlling sediment transports at the mouth of a highly energetic inlet system (San Francisco Bay, CA). *Marine Geology*. <http://dx.doi.org/10.1016/j.margeo.2012.07.003>.
- Fram, J.P., 2005. Exchange at the estuary-ocean interface: Fluxes through the golden gate channel. Ph.D. dissertation, University of California, Berkeley.
- Fram, J., Martin, M., Stacey, M., 2007. Dispersive fluxes between the coastal ocean and semi-enclosed estuarine basin. *Physical Oceanography* 1645–1660.
- Ganju, N., Schoellhamer, D., 2006. Annual sediment flux estimates in a tidal strait using surrogate measurements. *Estuarine, Coastal and Shelf Science* 69, 165–178.
- Ganju, N., Schoellhamer, D., 2009. Calibration of an estuarine sediment transport model to sediment fluxes as an intermediate step for simulation of geomorphic evolution. *Continental Shelf Research* 29, 148–158.
- Gartner, J.W., 2004. Estimating suspended solids concentrations from backscatter intensity measured by acoustic Doppler current profiler in San Francisco Bay, California. *Marine Geology* 211, 169–187.
- Hauck, L., Teeter, A., Pankow, W., Evans, R.J., 1990. San Francisco Bay suspended sediment movement: report I: summer condition data collection and numerical model verification. Technical Report HL-90-6. U.S. Army Engineer Waterways Experiment Station, Vicksburg, MS.
- Jaffe, B.E., Smith, R., Foxgrover, A., 2007. Anthropogenic influence on sedimentation and intertidal mudflat change in San Pablo Bay, California: 1856–1983. *Estuarine, Coastal and Shelf Science* 73, 175–187.
- Kineke, G., Sternberg, R., 1989. The effect of particle settling velocity on computed suspended sediment concentration profiles. *Marine Geology* 90, 159–174.
- Krank, K., Milligan, T., 1992. Characteristics of suspended particles at an 11-hour anchor station in San Francisco Bay, California. *Journal of Geophysical Research* 97 (C7), 11373–11382.
- Kroll, G., 1975. Estimate of Sediment Discharges, Santa Ana River at Santa Ana and Santa Maria River at Guadalupe California. U.S. Geological Survey, s.l.
- Krone, R., 1962. Flume Studies of the Transport of Sediment in Estuarial Shoaling Processes. U.C. Berkeley, Berkeley.
- Largier, J., 1996. Hydrodynamic exchange between San Francisco Bay and the ocean: the role of ocean circulation and stratification. San Francisco Bay: the ecosystem. AAAS, s.l. pp. 69–104.
- Lesser, G.R., Roelvink, J.A., van Kester, J.A.T.M., Stelling, G.S., 2004. Development and validation of a three-dimensional morphological model. *Coastal Engineering* 51 (8–9), 883–915.
- Locke, J.L., 1971. Sedimentation and Foraminiferal Aspects of the Recent Sediments of San Pablo Bay. (M.S. thesis) San Jose State University, San Jose, CA (100 pp.).
- Martin, M.A., Fram, J.P., Stacey, M.T., 2007. Seasonal chlorophyll a fluxes between the coastal Pacific Ocean and San Francisco Bay. *Marine Ecology Progress Series* 337, 51–61.
- McKee, L., Ganju, N., Schoellhamer, D., 2006. Estimates of suspended sediment entering San Francisco bay from the Sacramento and San Joaquin Delta, San Francisco Bay, California. *Journal of Hydrology* 323, 335–352.
- McKee, L.J., Lewicki, M., Schoellhamer, D.H., Ganju, N.K., 2013. Comparison of sediment supply to San Francisco Bay from watersheds draining the Bay Area and the Central Valley of California. *Marine Geology* 345, 47–62 (this issue).
- Mehta, A., 1986. Laboratory studies on cohesive sediment deposition and erosion. In: Dronkers, J., van Leussen, W. (Eds.), *Physical Processes in Estuaries*. Springer Verlag, New York.
- Monosmith, S., Kimmerer, W., Burau, J., Stacey, M., 2002. Structure and flow-induced variability of the subtidal salinity field in Northern San Francisco Bay. *Journal of Physical Oceanography* 32, 3003–3019.
- Ogden Beeman and Associates, I., 1992. Sediment Budget for San Francisco Bay: Final Report. U.S. Army Engineer District, San Francisco.
- Parker, D., Norris, D., Nelson, A., 1972. Tidal Exchange at the Golden Gate. ASCE, s.l. 305–323.
- Pawlowicz, R., Beardley, B., Lentz, S., 2002. Classical tidal harmonic analysis including error estimates in MATLAB using T\_TIDE. *Computers & Geosciences* 28, 929–937.
- Porterfield, G., 1980. Sediment Transport of Streams Tributary to San Francisco, San Pablo and Suisun Bays, California, 1909–66. U.S. Geological Society, s.l.
- Roelvink, J., 2006. Coastal morphodynamic evolution techniques. *Coastal Engineering* 53, 177–187.
- Rubin, D.M., McCulloch, D.S., 1979. The movement and equilibrium of bedforms in Central San Francisco Bay. In: Conomos, T.J. (Ed.), *The Urbanized Estuary*. American Association for the Advancement of Science, San Francisco Bay, pp. 97–113.
- Ruhl, C., Schoellhamer, D., Stumpf, R., Lindsay, C., 2001. Combined use of remote sensing and continuous monitoring to analyse the variability of suspended-sediment concentrations in San Francisco Bay, California. *Estuarine, Coastal and Shelf Science* 53, 801–812.
- Schoellhamer, D.H., 2011. Sudden clearing of estuarine waters upon crossing the threshold from transport- to supply-regulation of sediment transport as an erodible sediment pool is depleted: San Francisco Bay, 1999. *Estuaries and Coasts* 34, 885–899.
- Schoellhamer, D.H., Lionberger, M.A., Jaffe, B.E., Ganju, N.K., Wright, S.A., Shellenbarger, G.G., 2005. Bay Sediment Budgets: Sediment Accounting 101: The Pulse of the Estuary: Monitoring and Managing Water Quality in the San Francisco Estuary. San Francisco Estuary Institute, Oakland, California 58–63 (URL [http://www.sfei.org/rmp/pulse/2005/RMP05\\_PulseoftheEstuary.pdf](http://www.sfei.org/rmp/pulse/2005/RMP05_PulseoftheEstuary.pdf)).
- Schoellhamer, D.H., Wright, S.A., Drexler, J.Z., 2013. Adjustment of the San Francisco estuary and watershed to decreasing sediment supply in the 20th century. *Marine Geology* 345, 63–71 (this issue).
- Scripps Institution of Oceanography, 2012. The Coastal Data Information Program (CDIP), wave data. <http://cdip.ucsd.edu/>. Last accessed November 2012.
- Simpson, M.R., 2001. Discharge measurements using a broad-band acoustic Doppler current profiler. U.S. Geological Survey, Open-File Report 01-1.
- Singer, M.A.R., James, L., 2008. Status of the lower Sacramento Valley flood-control system within the context of its natural geomorphic setting. *Natural Hazards Review* 9, 104–115.
- Smith, L.H., 1987. A review of circulation and mixing studies of San Francisco Bay, California. U.S. Geological Survey Circular, 1015 (38 pp.).
- Talke, S., Stacey, M., 2003. The influence of oceanic swell on flows over an estuarine intertidal mudflat in San Francisco Bay. *Estuarine, Coastal and Shelf Science* 58, 541–554.
- Teeter, A., 1986. Alcatraz Disposal Site Investigation: Report 3: San Francisco Bay-Alcatraz Site Disposal Erodibility. U.S. Army Engineers Waterway Experiment Station, Vicksburg, MS.
- Teeter, A.M., Letter, J.V., Pratt, T.C., Callegan, C.J., Boyt, W.L., 1996. San Francisco Bay long-term management strategy (LTMS) for dredging and disposal. Report 2. Baywide suspended sediment transport modeling. Technical Report #A383413. Army Engineer Waterways Experiment Station, Hydraulics Lab, Vicksburg, MS.
- van der Wegen, M., Dastgheib, A., Jaffe, B., Roelvink, D., 2011a. Bed composition generation for morphodynamic modeling: case study of San Pablo Bay in California, USA. *Ocean Dynamics* 61, 173–186.
- van der Wegen, M., Jaffe, B., Roelvink, J., 2011b. Process-based, morphodynamic hindcast of decadal. *Journal of Geophysical Research* 116, 22.
- Van Rijn, L., 2007. Unified view of sediment transport by currents and waves. II: suspended transport. *Journal of Hydraulic Engineering* 133 (6), 668–689.
- Wintwerp, J., Van Kesteren, W., 2004. Introduction to the physics of cohesive sediment in the marine environment. *Developments in Sedimentology* 56.
- Wright, S., Schoellhamer, D., 2004. Trends in the sediment yield of the Sacramento River, California, 1957–2001. *San Francisco Estuary and Watershed Science* 2 (2), 14.
- Wright, S., Schoellhamer, D., 2005. Estimating sediment budgets at the interface between rivers and estuaries with application to the Sacramento–San Joaquin River Delta. *Water Resources Research* 41.
- Zedler, J., Callaway, J., 2001. Tidal wetland functioning. *Journal of Coastal Research Special Issue* 2001, 38–64.